Heating Titan's upper atmosphere

V. De La Haye,[1] J. H. Waite Jr.,[1] T. E. Cravens,[2] S. W. Bougher,[3] I. P. Robertson,[2] and J. M. Bell[1]

Received 6 February 2008; revised 11 August 2008; accepted 20 August 2008; published 19 November 2008.

[1] A detailed analysis of the mechanisms heating Titan's neutral atmosphere is provided. Two primary sources of incoming energy, the solar photons and the energetic electrons from Saturn's magnetosphere, are taken into account. The processes studied include the excitation of atmospheric molecules by electron impact, suprathermal electron heating, and the energy release through ion and neutral exothermic chemistry. The redistribution of heat by suprathermal particles throughout the atmosphere is also considered and calculated using a two-stream model. Local time-dependent heating rate profiles are presented. Exothermic chemistry is found to be the dominant source of heat, with electron-impact excitation and suprathermal electron heating becoming significant at high altitudes. Large variations in local peak amplitudes were found, varying between $\simeq 3 \times 10^{-10}$ erg cm^{-3}s^{-1} at 990 km and zenith angle 62° and $\simeq 7 \times 10^{-12}$ erg cm^{-3}s^{-1} at 940 km and zenith angle 165°. Neutral heating efficiency profiles averaged with respect to local time at the fixed latitudes of 38.8° N and 73.7° N are presented, with mean values of $\simeq$25 ± 15% and 23 ± 19%, respectively.

Citation: De La Haye, V., J. H. Waite Jr., T. E. Cravens, S. W. Bougher, I. P. Robertson, and J. M. Bell (2008), Heating Titan's upper atmosphere, *J. Geophys. Res.*, *113*, A11314, doi:10.1029/2008JA013078.

1. Introduction

[2] Heating efficiencies are traditionally defined as the fraction of the solar energy absorbed by the neutral atmosphere that appears as heat at a given altitude. Various assessments of the thermospheric heating efficiencies have been provided across the years for the case of the Earth. *Torr et al.* [1980], in particular, based their study on experimental measurements recorded over the preceding five years, especially the measurements of the incoming solar flux in the extreme ultraviolet and Schumann-Runge continuum. Then, solving the ionospheric continuity, momentum and energy equations, and modeling photoelectron transport using the two stream method of *Nagy and Banks* [1970], *Torr et al.* [1980] provided an evaluation of the amount of solar ultraviolet energy distributed amongst three major channels: radiation, dissociation of molecular oxygen, and kinetic heating of the particles in the thermosphere. They studied the energy going into heat at each altitude, and estimated the heating efficiency to vary between $\simeq$50% near the peak of the EUV energy deposition at about 175 km, and $\simeq$10% at about 400 km.

[3] A coupled thermosphere and ionosphere global average model was then constructed by *Roble et al.* [1987] for the Earth's thermosphere. Ten heating processes were taken into account, including absorption of solar UV radiation, heating by neutral-neutral and ion-neutral chemical reactions, heating by collisions between electrons, ions and neutrals, quenching of $O(^1D)$ by N_2 and O_2, atomic oxygen recombination, and heating by fast photoelectrons. This latter heating term, resulting from the impact of photoelectrons with the neutral gas, was assumed to represent 5% of the solar EUV energy absorbed. They found an overall neutral gas heating efficiency profile consistent with that of *Torr et al.* [1980], with a peak of 54% at $\simeq$155 km for solar minimum and 170 km for solar maximum.

[4] *Fox* [1988] provided an evaluation of the heating efficiencies for the thermosphere of Venus, and showed that the value of 10% used in thermospheric models could not be justified from a molecular point of view. Among mechanisms such as quenching, photodissociation, and exothermic chemical reactions, *Fox* [1988] estimated the fraction of the energy that appears as vibrational excitation and might subsequently be lost through radiation to space. Between 115 and 200 km, the resulting heating efficiency profiles were found to be in the range 16% to 25%. *Waite et al.* [1983] studied the thermosphere of Jupiter and found a neutral heating efficiency of 53% for solar EUV absorption and approximately 50% for a 10 keV electron precipitation.

[5] In Titan's upper atmosphere, two of the primary sources of incoming energy are solar photons and energetic electrons from Saturn's magnetosphere. The energy is first absorbed by the neutrals present in Titan's upper atmosphere, which become either excited, dissociated, or ionized. The energy is then redistributed either by suprathermal electrons, resulting from photoionization and electron impact ionization, or by exothermic reactions, involving Titan's complex neutral and ion chemistry (Figure 1). The exother-

[1]Southwest Research Institute, San Antonio, Texas, USA.
[2]Department of Physics and Astronomy, University of Kansas, Lawrence, Kansas, USA.
[3]Department of Atmospheric, Oceanic and Space Sciences, University of Michigan, Ann Arbor, Michigan, USA.

0148-0227/08/2008JA013078

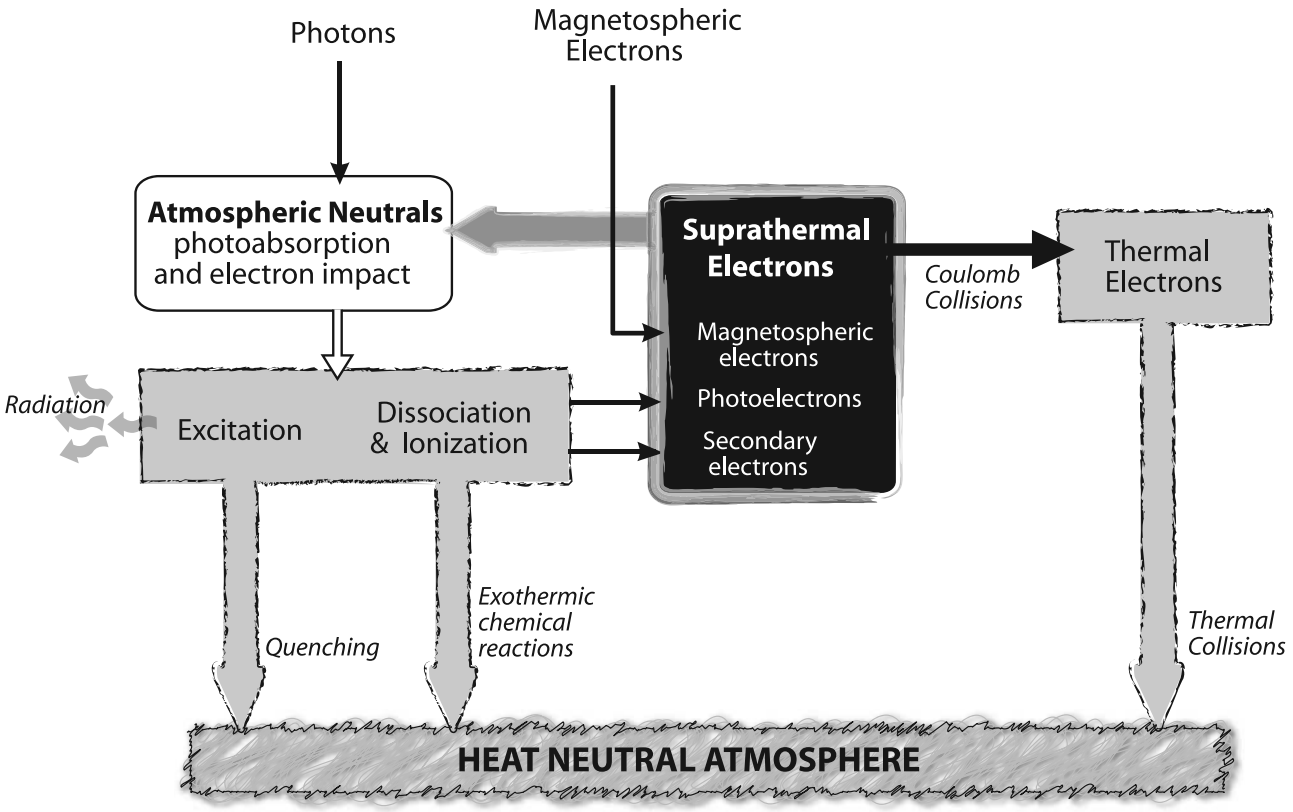

Figure 1. Heating processes in Titan's upper atmosphere induced by solar radiation and magnetospheric electrons.

mic chemical reactions may produce suprathermal particles, in which case the energy, instead of being directly released into the atmosphere, is redistributed vertically. In all cases, the energy path in Titan's upper atmosphere is tightly linked to the composition.

[6] *Friedson and Yung* [1984] provided succinct estimates of the heating efficiencies resulting from the absorption of solar radiation by methane for Titan. The three channels considered for the photodissociation of CH_4 were evaluated separately: (1) $CH_4 + h\nu \rightarrow {}^1CH_2 + H_2$, (2) $CH_4 + h\nu \rightarrow CH_2 + 2H$, and (3) $CH_4 + h\nu \rightarrow CH + H_2 + H$. The kinetic energy of the fragments produced in each channel, as well as the energy from the recombination of radicals CH_2 and CH producing new C_2H_2 molecules, were assumed to contribute to local heating. The average heating efficiency over the three photodissociation channels was estimated to be 35% at Lyman α, and to vary between 47% and 32% between 1000 Å and 1300 Å. Using a similar study, *Friedson and Yung* [1984] estimated an average heating efficiency of 45% after absorption of solar radiation by acetylene between 1300 Å and 2000 Å.

[7] Altitude-dependent heating efficiencies of Titan's thermosphere were shown in a presentation by *Fox and Yelle* [1991]. These heating efficiencies were determined for solar EUV radiation, at wavelengths between 14 and 2000 Å, using a daytime model of the ionosphere and thermosphere of Titan. The Voyager measurements were used for the density profiles of N_2 and CH_4, while the photochemical calculations of *Yung et al.* [1984] were used for the density profiles of C_2H_2, C_2H_4 and C_2H_6, and the densities of H_2, H, HCN, as well as all the major ions were determined as part of the model's calculations. The reactions resulting from solar processes and photoelectron impacts were taken into account in the heating rate calculations. The average heating efficiency was presented as $\simeq$27 ± 5% over the altitude range 800 to 1300 km; however, these results were never published.

[8] A detailed analysis of the mechanisms responsible for the heating of Titan's neutral atmosphere is carried on in the present work for altitudes between 600 and 1500 km, about 50 km higher than the exobase altitude estimated by *De La Haye et al.* [2007a]. Solar photons and the energetic electrons from Saturn's magnetosphere are considered as primary sources of incoming energy. Two heating mechanisms induced by suprathermal electrons are first studied using the model of *Gan et al.* [1992]: energy transfers with neutrals by elastic and inelastic collisions, and energy transfers with thermal electrons by Coulomb collisions. Heating induced by photochemistry is then detailed using the local time-dependent ion and neutral coupled model of *De La Haye et al.* [2008]. The present study takes into account the production and travel of suprathermal neutrals, using the two stream model of *De La Haye et al.* [2007b]. The resulting heating rates and heating efficiency profiles are presented.

[9] In addition to energy due to solar photons and magnetospheric electrons, there is also energy deposited in the atmosphere by energetic magnetospheric ions and pick up ions, particularly at altitudes between 500 and 1000 km [*Cravens et al.*, 2008]. The energy deposition due to

deflected magnetospheric N^+ ions and N_2^+ pickup ions was calculated by *Michael and Johnson* [2005], using a Direct Simulation Monte Carlo method. They concluded that energy deposition by pickup ions near the exobase was greater than solar radiation, but found a maximum temperature increase near the exobase of only a few Kelvins (4 to 7 K). Thus, although it was shown that magnetospheric and pickup ions represent an important energy source for Titan's upper atmosphere, determining its efficiency at actually heating Titan's neutral atmosphere will require further study, and a better understanding of the complex interaction between Saturn's magnetosphere and Titan's complex ion and neutral chemistry. This work is outside the scope of the present study.

2. Two Heating Mechanisms Induced by Suprathermal Electrons

[10] The electron flux reaching Titan's upper atmosphere is composed of two types of primary electrons: the photoelectrons, resulting from the photoionization of neutrals, and the magnetospheric electrons coming from Saturn's magnetosphere and penetrating Titan's upper atmosphere by following the magnetospheric field lines. These primary electrons interact with Titan's atmosphere by heating, exciting, and ionizing the local neutral particles. The electron-induced ionizations lead to the production of secondary electrons (Figure 1).

[11] The electron fluxes were separately computed with the model of *Gan et al.* [1992]. This model was constructed in two interdependent parts: an electron energy code modeling the population of thermal electrons (low energy $\simeq 0.01$ eV, thermalized with the neutral atmosphere), and a two stream transport code to model the suprathermal electron upward and downward fluxes (high energy $\simeq 1$ eV to 100 eV), as well as the partitioning of energy amongst the various loss processes.

[12] The present section examines two heating mechanisms of Titan's neutral atmosphere by suprathermal electrons, including photoelectrons, magnetospheric electrons, and secondary electrons. The first process involves neutrals' excitation by collisional impact with suprathermal electrons. (Electron impact dissociation and ionization are taken into account in the following section on photochemistry). And the second process involves Coulomb collisions between suprathermal electrons and thermal electrons.

2.1. Excitation of Neutrals by Collisional Impacts With Suprathermal Electrons

2.1.1. Excitation of Molecular Nitrogen

[13] Following electron impact, the energy of the electron is transferred to the nitrogen molecules in the form of kinetic energy (elastic collision) and internal excitation (inelastic collision), including vibrational excitation and electronic excitation. These internal excited states may lead to the ionization and dissociation of N_2 (see section 3).

[14] For the vibrational excitation of N_2, cross sections are determined using the following analytical expression:

$$\sigma_s(E) = \frac{q_0 f_0 C_{0,s}}{W_s^2}\left(\frac{W_s}{E}\right)^{\Omega_s}\left(1-\left(\frac{W_s}{E}\right)^{\beta_s}\right)^{\nu}, \qquad (1)$$

where $\nu_{N_2} = 1.58$, $\Omega_{N_2} = 8.0$, $W_{N_2} = 1.85$, $f_0 C_{0,N_2} = 1.35$, and $\beta_{N_2} = 1.0$ are the Generalized Optical Strength (G.O.S.) parameters for N_2, and where $q_0 = 4\pi a_0^2 R^2 = 6.514 \times 10^{-14}$ eV^{2}cm^2, with a_0 and R being the Bohr radius and the Rydberg energy constant, respectively [*Gan*, 1991; *Green and Dutta*, 1967]. Owing to the cold temperature of Titan's upper atmosphere, most of the vibrationally excited N_2 molecules resulting from electron impact are assumed to be in the first vibrational level $v = 1$, with an energy of $E_v = 0.435$ eV determined using the expression of *Herzberg* [1950]:

$$E_v = hc\omega_e\left(v+\frac{1}{2}\right) - hc\omega_e x_e\left(v+\frac{1}{2}\right)^2 + hc\omega_e y_e\left(v+\frac{1}{2}\right)^3, \quad (2)$$

where $\omega_e = 2359.61$ cm^{-1}, $\omega_e x_e = 14.456$ cm^{-1}, and $\omega_e y_e = 0.00751$ cm^{-1}. It is assumed that the energy of the nitrogen first vibrational level is quenched by the ions and neutrals present, and eventually leads to the heating of the neutral atmosphere.

[15] The following N_2 electronic excitation states are considered: A, B, B', W, C, a, a', w, b', and the sums of the $^1\Pi_u$ and Rydberg electronic excited states. The corresponding cross sections are chosen to be the same as these used by *Gan et al.* [1992] [*Gan*, 1991; *Cartwright et al.*, 1977; *Trajmar et al.*, 1983; *Zipf and McLaughlin*, 1978; *Green and Sawada*, 1972]. They are compared in Figure 2 with the vibrational cross sections, the ionization and dissociation cross sections [*De La Haye et al.*, 2008; *Zipf et al.*, 1980; *Itikawa et al.*, 1986], and the elastic differential cross sections [*Gan*, 1991; *Trajmar et al.*, 1983; *Solomon et al.*, 1988]. In *Gan et al.* [1992], the electron impact cross sections for the sum of the Rydberg states added to the sum of the $^1\Pi_u$ states and to the b' state were normalized to reproduce the total dissociation cross section of *Zipf and McLaughlin* [1978]. These excited states are also assumed here to solely result in dissociation. The contribution of the kinetic and internal energy of the dissociated products, a combination of $N(^4S, ^2D, ^2P)$, is studied in the following section.

[16] Further considerations are needed to calculate the heating involving excited states $A(^3\Sigma_u^+)$, $B(^3\Pi_g)$, $W(^3\Delta_u)$, $B'(^3\Sigma_u^-)$, $a'(^1\Sigma_u^-)$, $a(^1\Pi_g)$, $w(^1\Delta_u)$, and $C(^3\Pi_u)$. First, the most probable vibrational level for each of these electronic excited states is determined using the Franck Condon factors. According to the Franck-Condon principle, the electron jump occurring during the electronic excitation of a molecule takes place so rapidly that the internuclei distance remains close to the same immediately afterward. Further, since the equilibrium internuclear distance is different in the new electronic state, the nuclei start vibrating. The Franck Condon factors represent the square of the overlap integral between the wave functions, and are proportional to the probability for a molecule to make a transition $v'' \rightarrow v'$. Although several vibrational levels compete closely for each excitation state, only the maximal Franck Condon factor is taken into account in the present study. Using the Franck Condon factors of *Gilmore et al.* [1992], the most probable vibrational levels are found to be $v' = 8$, 2, 7, 7, 7, 3, 6, and 0 for states A, B, W, B', a', a, w, and C, respectively.

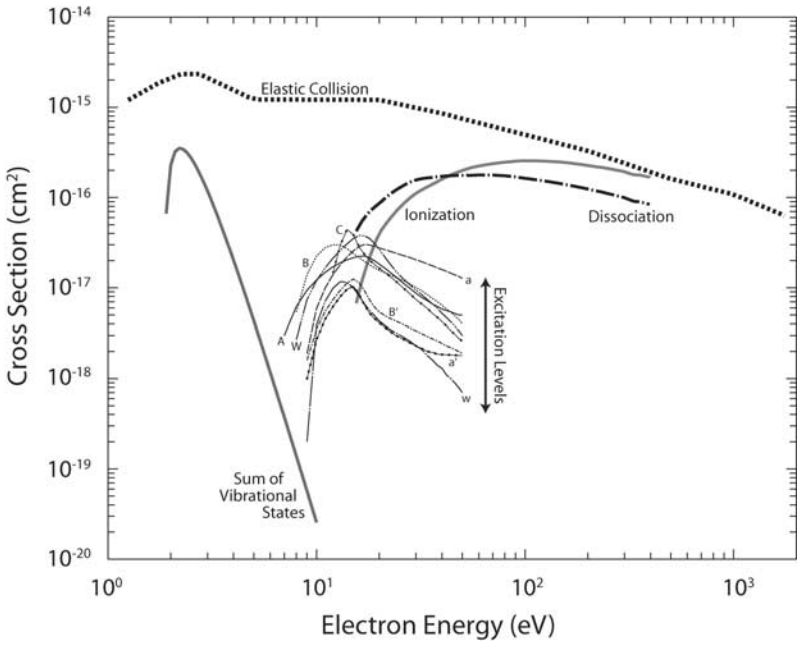

Figure 2. Electron impact cross sections for elastic collision, vibrational excitation, ionization, and dissociation of N_2.

[17] The radiative lifetimes and quenching coefficients for excited states A, B, W, B', a', a, w, and C are compared in Table 1. Excitation thresholds and main observed transitions are also displayed. The quenching time constant is estimated by assuming N_2 as main quencher with a density of 10^{13} cm^{-3}, corresponding to an altitude of 600 km, i.e., the denser part of the atmosphere for the altitude range of the present study. For all excited states, the quenching mechanisms are found to be at least one order of magnitude slower than radiation at 600 km. The possibility of energy release through quenching is therefore assumed to be negligible.

[18] In order to make a relevant estimate of the atmospheric heating resulting from excitation into electronic states A, B, W, B', a', a, w, and C, the radiative cascades initiated by each of these states in their most probable

Table 1. Radiative Lifetimes and Quenching Rates for Some of the Molecular Nitrogen Electronic Excited States

Excited States	Threshold[a] (eV)	Observed Transitions[b]	Radiative Lifetime (s)	Ref.[c]	Quenching Rate by N_2 (cm^{3}s^{-1})	Quenching Time[d] (s)	Ref.
$N_2(A)$	6.1693	$A \rightarrow X$	2.05 ($v' = 0$)	1	10^{-19}	10^{6}	2
			1.99 ($v' = 8^e$)	1			
			$\simeq$2 ($v' = 0$)	2			
$N_2(B)$	7.3529	$B \rightarrow A$	$(6.5 \pm 1.5) \times 10^{-6}$ ($v' = 0$)	3	3×10^{-11}	3.33×10^{-3}	5
			1.13×10^{-5} ($v' = 0$)	1			
			9.26×10^{-6} ($v' = 2^e$)	1			
$N_2(W)$	7.3623	$W \leftrightarrow B$	$>1^f$ ($v' = 0$)	1	1.72×10^{-11g}	5.8×10^{-3}	8
			1.61×10^{-4} ($v' = 7^e$)	1			
$N_2(B')$	8.1647	$B' \leftrightarrow B$	4.54×10^{-5} ($v' = 0$)	1	8.49×10^{-12g}	1.18×10^{-2}	8
			1.76×10^{-5} ($v' = 7^e$)	1			
$N_2(a')$	8.3987		$2.3^{+1.1}_{-0.6} \times 10^{-2}$($v' = 0$)	4	$(1.9 \pm 0.5) \times 10^{-13}$	5.26×10^{-1}	4
$N_2(a)$	8.5489	$a \rightarrow a', X$	$(1.15 \pm 0.46) \times 10^{-4}$ ($v' = 0$)	3	$(2.2 \pm 0.2) \times 10^{-11}$	4.5×10^{-3}	6
			5.77×10^{-5} ($v' = 0$)	1			
			5.5×10^{-5} ($v' = 3^e$)	1			
$N_2(w)$	8.8948	$w \leftrightarrow a$	7.67×10^{-4} ($v' = 0$)	1	$(2.6 \pm 0.2) \times 10^{-11h}$	3.8×10^{-3}	9
			1.26×10^{-4} ($v' = 6^e$)	1			
$N_2(C)$	11.0316	$C \rightarrow B$	$(4.1 \pm 0.29) \times 10^{-8}$ ($v' = 0$)	3	5.75×10^{-12}	1.74×10^{-2}	7
			3.71×10^{-8} ($v' = 0^e$)	1	(3.7×10^{-4} ns^{-1} torr^{-1})		

[a] *Cartwright et al.* [1977].
[b] *Herzberg* [1950]; *Gilmore et al.* [1992]; *Eastes and Dentamaro* [1996].
[c] 1, *Gilmore et al.* [1992]; 2, *McEwan and Phillips* [1975]; 3, *Khristenko et al.* [1998]; 4, *Piper* [1987]; 5, *Piper* [1992]; 6, *Marinelli et al.* [1989]; 7, *Millet et al.* [1973]; 8, *Morrill and Benesh* [1996]; 9, *Eastes and Dentamaro* [1996] and *Katayama et al.* [1994].
[d] The quenching times were estimated from the quenching rates by considering a N_2 density of 10^{13}cm^{-3}, which corresponds to $\simeq$600 km in Titan's upper atmosphere.
[e] Vibrational state the most probable determined using the Franck Condon factors listed by *Gilmore et al.* [1992].
[f] The value strongly depends on the spin component and rotational level.
[g] The quenching rates were determined for the collisional transfers from $N_2(B)$ to $N_2(W)$ and $N_2(B')$, as part of a study on the $B \leftrightarrow A$, $B' \leftrightarrow B$, $W \leftrightarrow B$ intrasystem cascade, and are only reported here for reference.
[h] The $w \leftrightarrow a$ collisional rate is approximated as that of $a \leftarrow a'$ as suggested by *Eastes and Dentamaro* [1996].

Table 2. Estimated Fractions of the Energy Thresholds of the N_2 Electronic Excited States Used to Heat Neutrals in Titan's Upper Atmosphere

Excited States	Heat Fraction	Excited States	Heat Fraction
$N_2(A)$	0%	$N_2(a')$	0%
$N_2(B)$	30.9%	$N_2(a)$	0%
$N_2(W)$	33.3%	$N_2(w)$	0%
$N_2(B')$	32.1%	$N_2(C)$	18.1%

vibrational level are considered from the lower- to the higher-energy state, using the Einstein coefficients determined by *Gilmore et al.* [1992]. The case of $N_2(B, v' = 2)$ is presented here as an example.

[19] In studying the fastest radiative transitions between excited states $N_2(B, v' = 2)$ and $N_2(A, v'')$, two spontaneous emissions of equivalent importance are taken into account [*Gilmore et al.*, 1992]:

$$N_2(B, v' = 2) \rightarrow N_2(A, v'' = 0), \; A_{v',v''} = 4.29 \times 10^4 s^{-1}, \quad (3)$$

$$N_2(B, v' = 2) \rightarrow N_2(A, v'' = 1), \; A_{v',v''} = 5.54 \times 10^4 s^{-1}, \quad (4)$$

In the first case, the radiative cascade leads from $N_2(A, v' = 0)$ to $N_2(X, v'' = 6)$, identified as the fastest transition with an Einstein coefficient of $A_{v',v''} = 1.02 \times 10^{-1} s^{-1}$ [*Gilmore et al.*, 1992]. It is then assumed that the excited state $N_2(X, v'' = 6)$ is quenched by the background gas, and that the corresponding vibrational energy, $E_v = {}_6 = 1.826$ eV (equation (2)), is used as heat source for Titan's upper atmosphere. In the second case, the fastest spontaneous energy transfer is found to lead from $N_2(A, v' = 1)$ to $N_2(X, v'' = 9)$, with an Einstein coefficient of $A_{v',v''} = 1.05 \times 10^{-1} s^{-1}$ [*Gilmore et al.*, 1992]. As in the first case, the energy of this ground state vibrational level, $E_v = {}_9 = 2.618$ eV, is assumed to be released as heat into the atmosphere.

[20] The same method is applied to excited states $(A, v' = 8)$, $(W, v' = 7)$, $(B', v' = 7)$, $(a', v' = 7)$, $(a, v' = 3)$, $(w, v' = 6)$, and $(C, v' = 0)$. The resulting portions of the N_2-electronic excited energy used to heat Titan's upper atmosphere are listed in Table 2, with estimates varying between 0% and 30%.

2.1.2. Excitation of Methane

[21] After impact, the energy of the suprathermal electrons is transferred to methane molecules as kinetic energy (elastic collisions) and internal excitation (inelastic collisions), including vibrational excitation, rotational excitation, and electronic excitation. In the present study, the cross sections corresponding to these four processes are the same as those used in the model of *Gan et al.* [1992] [*Gan*, 1991; *Jain and Thomson*, 1983; *Jain*, 1986; *Shyn and Cravens*, 1990; *Tanaka et al.*, 1983; *Sohn et al.*, 1983; *Shimamura*, 1983; *Muller et al.*, 1985; *Brescansin et al.*, 1989]. They are plotted in Figure 3, where they are compared with the ionization cross sections of *Orient and Srivastava* [1987], used in the coupled ion and neutral model of *De La Haye et al.* [2008]. The ionization and dissociative ionization of CH_4 by electron impact are studied in the following section.

[22] The dominant vibrational excitation processes involve vibrational levels ν_1, ν_2, ν_3, and ν_4. These four vibrational states were taken into account by *Gan* [1991] and *Gan and Cravens* [1992] as two combined processes $\nu_{1,3}$ with threshold 0.367 eV and $\nu_{2,4}$ with threshold 0.175 eV. The totality of the energy involved in these vibrational states is assumed to become eventually quenched and used as a heat source for Titan's upper atmosphere.

[23] In the case of the rotational excitation of methane, not all angular momentum values are allowed. According to *Gan* [1991], *Gan and Cravens* [1992], and *Herzberg* [1945], the rotational levels $J = 1, 2, 5$ cannot be reached

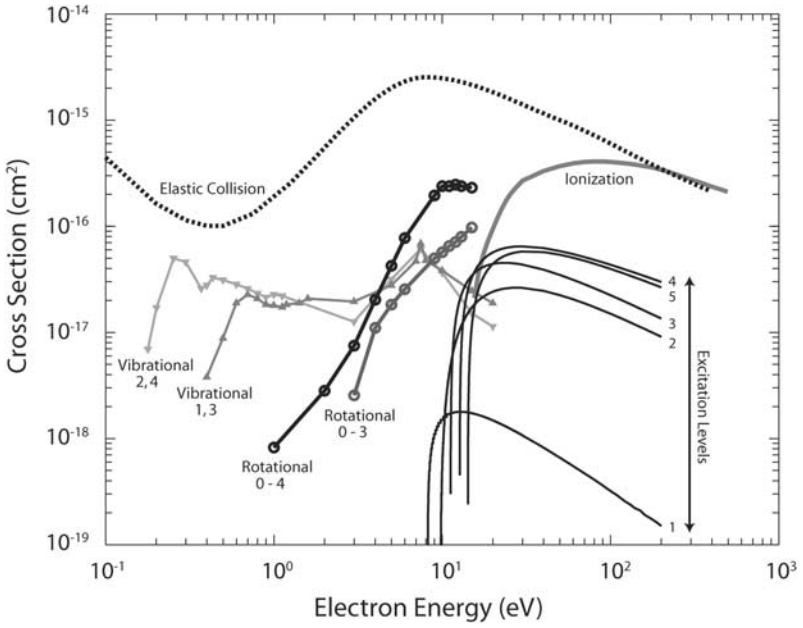

Figure 3. Electron impact cross sections for elastic collision, ionization, vibrational, rotational, and electronic excitation of CH_4.

owing to the geometric characteristics of CH_4 and to its spin statistics. In addition, the transition to larger angular momentum ($J \geq 6$) is unlikely owing to the centrifugal barrier preventing the wave function from becoming large close to the molecule. Therefore, the present study was restricted to the rotational excitation levels $J = 0, 3, 4$. As suggested by *Gan* [1991] and *Gan and Cravens* [1992], the theoretical values of *Jain and Thomson* [1983] are adopted for the rotational excitation cross sections and multiplied by a factor of 2 in order to match other experimental measurements (Figure 3). As rotational excitation levels are estimated to be rapidly thermalized, their energy E_J is assumed to contribute to direct heating of Titan's neutral atmosphere:

$$E_J = hcBJ(J+1), \tag{5}$$

where E_J is the energy of rotational level $J = 3, 4$, h is the Planck constant, c is the speed of light, and $B = 5.24059\ \mathrm{cm}^{-1}$ is the methane rotational constant [*Susskind*, 1973].

[24] The present study uses the electronic excitation cross sections of methane estimated by *Gan* [1991] and *Gan and Cravens* [1992], based on a study by *Vuskovic and Trajmar* [1983], in which cross sections were measured at 20, 30 and 200 eV, for excitation levels previously divided into five energy channels: 7.5 to 9.0 eV, 9.0 eV to 10.5 eV, 10.5 to 12.0 eV, 12.0 to 13.5 eV, and 13.5 to 15.0 eV. *Gan* [1991] and *Gan and Cravens* [1992] showed that the energy-dependent excitation cross sections could be fitted with equation (1), and calculated the adapted Generalized Optical Strength (G.O.S) parameters for the five aforementioned energy levels. Since limited information is found in the literature on methane electronic excitation, it is assumed here that half of the excitation energy is radiated away, and half is used to efficiently heat Titan's neutral atmosphere. The results are not significantly affected since the quenching of electronically excited methane is not a major heating process. Further studies would be required to provide a more accurate estimate.

[25] The G.O.S. parameters were also estimated by *Gan and Cravens* [1992] for dissociative excitation of methane. However, the excited hydrogen atoms resulting from this process were found to produce airglow emissions in the extreme ultraviolet [*Vroom and de Heer*, 1969]. This last mechanism is assumed to be inefficient for heating the neutral atmosphere, and is neglected in the neutrals' energy balance.

2.1.3. Heating Rates Resulting From the Excitation of Nitrogen and Methane Molecules by Electron Impact

[26] The heating terms H_{is} resulting from the excitation of N_2 and CH_4 after impact with suprathermal electrons, are calculated using the following expression:

$$H_{is} = \epsilon_{is} E^*_{is} n_s \int_E \sigma_{is}(E) \Phi_{electron}(E) dE, \tag{6}$$

where σ_{is} is the cross section associated with species s (N_2 or CH_4) in the excited state i (electronic, vibrational, or rotational excitation), E^*_{is} is the energy of that excited state, ϵ_{is} is the fraction of E^*_{is} used to heat the neutral atmosphere (see previous section), n_s is the density of species s calculated using the local time-dependent composition of *De La Haye et al.* [2008], and $\Phi_e(E)$ is the flux of electrons with energy E (photoelectrons or magnetospheric electrons) calculated with the model of *Gan et al.* [1992].

[27] The model of *Gan et al.* [1992] was recently modified to match the solar conditions of the Cassini flybys and the nitrogen and methane density data recorded by the INMS instrument [*Waite et al.*, 2005; *De La Haye et al.*, 2007a]. Various runs were performed for the photoelectron flux, matching the set of zenith angles used in the model of *De La Haye et al.* [2008] to describe daily rotation: between 61.7° at noon and 164.8° at midnight for a fixed latitude of 38.8°N, corresponding to the closest approach of the Cassini Orbiter during flyby T_A, and between 97.0° at noon and 129.0° at midnight for a fixed latitude of 73.7°N corresponding to the closest approach of flyby T_5. The subsolar latitude was 23° S for both the T_A and T_5 flybys.

[28] For magnetospheric electrons, field line draping around Titan was taken into account by assuming parabolic magnetic field lines, anchored at 725 km with the apex placed at the subsolar point for the T_A simulation. Parabolic-shaped field lines were also used by *Gan et al.* [1992, 1993] and were shown by Magneto-Hydrodynamics simulations (MHD) to represent a reasonable approximation for the field configuration [*Ma et al.*, 2004; *Ledvina and Cravens*, 1998]. The magnetospheric flux was assumed to be constant with local time due to the synchronous orbit of Titan around Saturn, with conditions corresponding to the magnetospheric wake. The magnetospheric electron population in the outer magnetosphere of Saturn is quite variable but has typical densities of about 0.5 cm^{-3} and thermal energies of about 200 eV, as measured by Voyager [*Neubauer et al.*, 1984] and by the Electron Spectrometer (ELS) of the Cassini Plasma Spectrometer (CAPS) [*Coates et al.*, 2007]. A statistical study of the CAPS ELS electron fluxes has not been undertaken to our knowledge, but the average fluxes and average energy for the outer magnetosphere near the T_5 Titan encounter appears to be quite a bit larger than for the T_{21} pass. Another issue that is far from being understood and outside the scope of the current paper is what fraction of the incident magnetospheric electron fluxes actually make it into the ionosphere itself [*Gan et al.*, 1992, 1993; *Agren et al.*, 2007]. The present paper adopts what appears to be the typical population just mentioned above, with an electron energy spectrum similar to that presented by *Agren et al.* [2007]. Heating efficiencies related to the magnetospheric electron inputs are estimated, which should allow future researchers to infer neutral heating rates for different magnetospheric electron inputs without having to recalculate atomic and molecular efficiencies.

[29] The heating rates obtained at a zenith angle of 60° are presented in Figure 4 for the photoelectrons and magnetospheric electrons. Comparison is provided between the effects of the N_2 and CH_4 elastic collisions, the N_2 electronic and vibrational excitations, and the CH_4 electronic, vibrational, and rotational excitations. Although atmospheric heating only takes place in the collisional region below the exobase (<1500 km), profiles are presented here up to 2000 km for reference. Heating resulting from the electronic excitation mechanisms is found to be the governing mechanisms both for the photoelectrons and for the magnetospheric electrons, with a predominance of the N_2 electronic excitation in the collisional region.

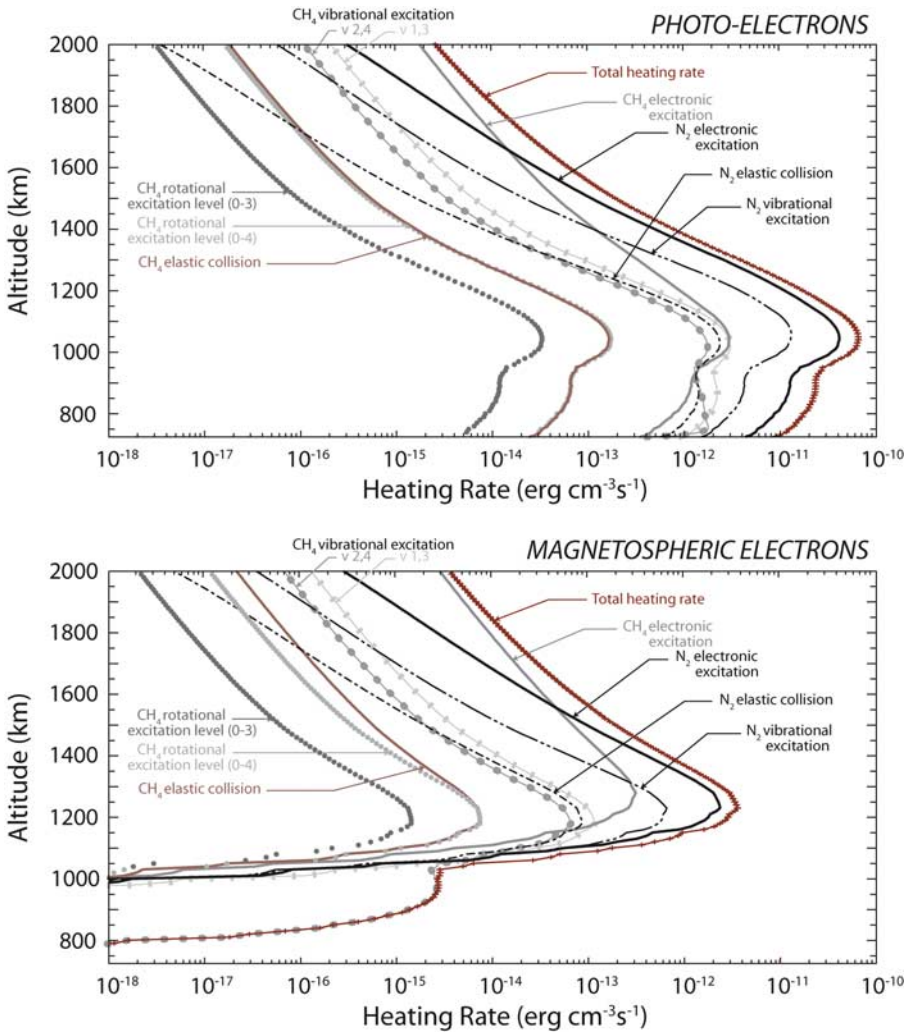

Figure 4. Heat released into Titan's atmosphere through elastic and excitational processes after collisions of (top) photoelectrons and (bottom) magnetospheric electrons with N_2 and CH_4, using a solar zenith angle of 60°.

[30] In addition, if one observes the heating rates produced by magnetospheric electrons alone, the heating coming from the excitation of CH_4 in vibrational state $v_{2,4}$ is the most distinctive profile below 1000 km. Referring to Figure 3, vibrational state $v_{2,4}$ stands out with an especially large electron impact cross section at very low electron energies (<0.4 eV). These low-energy electrons represent the only significant population of magnetospheric electrons reaching altitudes as low as 750 km in Titan's atmosphere. They are thus responsible for exciting the CH_4 molecules into vibrational state $v_{2,4}$, and instigate the local maximum of the heating rate observed at ≃950 km. This effect, however, is masked when considering the influence of photoelectrons, due to the presence at low altitude of a significant number of electrons transporting higher energies, which are able to excite electronically and vibrationally the atmospheric molecules, and are thereby more efficient sources of heat.

[31] The total heat released at a zenith angle of 60° into Titan's upper atmosphere through elastic collisions and excitation processes by suprathermal electrons is found to peak at 1040 km with a value of $\simeq 6.5 \times 10^{-11}$ erg cm^{-3}s^{-1} due to photoelectrons, and at 1230 km with a value of $\simeq 3.6 \times 10^{-12}$ erg cm^{-3}s^{-1} due to magnetospheric electrons.

2.2. Suprathermal Electron Heating

[32] The suprathermal electrons also interact with the population of thermal electrons, but via Coulomb collisions, including the effects of Coulomb electric field forces and Debye shielding. Coulomb collisions represent one of the major heat sources for the thermal electrons [*Gan et al.*, 1992]. The energy put into the thermal electrons is then assumed to be almost entirely transferred to the neutral gas via elastic, rotational, and vibrational cooling processes. However, thermal electrons and neutrals are not in thermal equilibrium, and the electron temperature remains well above the neutral temperature anywhere above about 1000 km [*Gan et al.*, 1992; *Galand et al.*, 2006; *Schunk and Nagy*, 2000]. The neutral heat source induced by Coulomb collisions between suprathermal electrons and thermal electrons is referred to in the text as suprathermal electron heating.

[33] The suprathermal electron heating rates were calculated using the recently modified version of the 2-stream

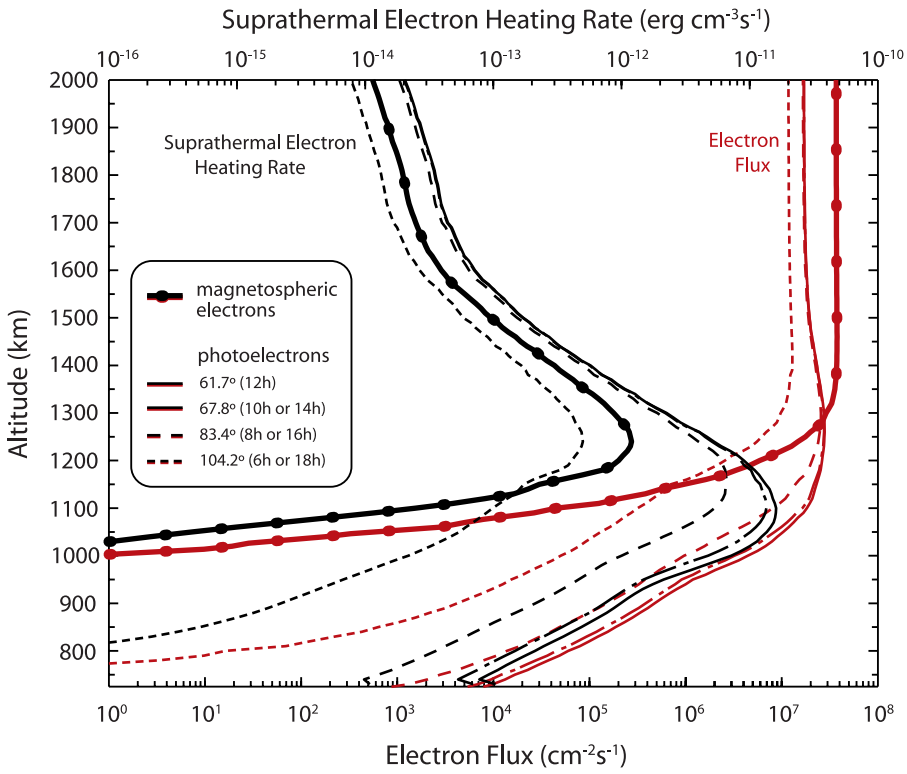

Figure 5. Suprathermal electron heating rates and electron fluxes computed with the model of *Gan et al.* [1992] for the array of zenith angles corresponding to the T_A simulation.

electron transport and electron energy model of *Gan et al.* [1992]. The resulting heating rates and corresponding electron fluxes, with all energy bins summed, are presented in Figure 5 for the local times and zenith angles corresponding to a daily rotation at latitude 38.8° North (T_A flyby conditions). When local time varies from day side to night side, the heating rate peaks due to photoelectrons are found to increase in altitude and decrease in amplitude. For example, the peak heat released into the atmosphere is found to be $\simeq 1.7 \times 10^{-11}$ erg cm^{-3}s^{-1} at 1100km for a zenith angle of 61.7°, $\simeq 6.8 \times 10^{-12}$ erg cm^{-3}s^{-1} at 1180 km for a zenith angle of 83.4°, and $\simeq 5.1 \times 10^{-13}$ erg cm^{-3}s^{-1} at 1240 km for a zenith angle of 104.2°. The heating rate peak due to magnetospheric electrons, $\simeq 1.2 \times 10^{-12}$ erg cm^{-3}s^{-1} at 1240 km, is dominated by the photoelectron effect on the day side. However, for zenith angles between 90 and 100°, the magnetospheric effect becomes predominant over the solar-driven processes, and represents the sole source of suprathermal electron heating throughout the rest of the night.

3. Heating Produced by Photochemistry

[34] The complex ion and neutral chemistry cascading from the photoionization, photodissociation, and electron impact ionization and dissociation of N_2 and CH_4 represent an important source of heat for Titan's neutral atmosphere. The energy contributions of excited particles, ion and neutral exothermic chemical reactions, and fragments from photodissociation, photoionization, and electron impact dissociation and ionization are evaluated in this section using the *De La Haye et al.* [2008] model. Local time-dependent heating rate profiles are estimated, taking into account energy redistribution by suprathermal neutrals resulting from exothermic chemistry.

3.1. Contribution of the Photochemical Model's Excited Particles

[35] The excited states $N(^2D)$ and $N(^2P)$ of atomic nitrogen are produced by photodissociation and electron impact dissociation of molecular nitrogen, and through electron recombination of the ion N_2^+. They have a very different effect on the energy balance of Titan's neutral atmosphere. First, the radiative lifetime of $N(^2P)$ is short, with a value of about $\simeq$12 s [*McEwan and Phillips*, 1975]. $N(^2P)$ becomes rapidly de-excited by radiating away its energy either down to the first excited level $N(^2D)$, with effective transition probability 7.9×10^{-2} s^{-1}, or directly down to the ground level $N(^4S)$, with effective transition probability 5.4×10^{-3} s^{-1} [*Zipf et al.*, 1980; *Chamberlain*, 1961]:

$$N\left(^2P\right) \overset{94\%}{\rightarrow} N\left(^2D\right) + h\nu(\lambda = 10,400\,\text{Å}), \tag{7}$$

$$N\left(^2P\right) \overset{6\%}{\rightarrow} N\left(^4S\right) + h\nu(\lambda = 3,446\,\text{Å}). \tag{8}$$

The quenching rate of $N(^2P)$ with N_2 was reported to be 3×10^{-19} cm^{3}s^{-1} [*McEwan and Phillips*, 1975]. Quenching of $N(^2P)$ is therefore a process several orders of magnitude slower than radiation in the thermosphere and mesosphere, and was neglected. Through channel (8), $N(^2P)$ represents a sink of energy for the neutral atmosphere. Its contribution to heating Titan's atmosphere depends on channel (7), the

dominant channel, and on the outcome of excited state $N(^2D)$.

[36] Excited state $N(^2D)$ was reported to be a long-lived state with a radiative lifetime of 9.36×10^4 s [*McEwan and Phillips*, 1975], which is comparable or slower than quenching time constants. For example, the quenching rate of $N(^2D)$ by N_2 is 1.6×10^{-14} cm^{3}s^{-1} [*Wilson and Atreya*, 2004; *Lin and Kaufman*, 1971]. It is assumed that $N(^2D)$ contributes to heating Titan's neutral atmosphere through the following quenching mechanisms:

$$\begin{aligned} N(^2D) + N_2 &\rightarrow N(^4S) + N_2\,(+2.38eV),\\ N(^2D) + C_2H_4 &\rightarrow CH_3CN + H\,(+2.43eV),\\ N(^2D) + C_2H_2 &\rightarrow CHCN + H\,(+1.06eV),\\ N(^2D) + CH_4 &\rightarrow NH + CH_3\,(+1.11eV),\\ N(^2D) + CH_4 &\rightarrow CH_2NH + H\,(+0.51eV),\\ N(^2D) + H_2 &\rightarrow NH + H\,(+1.12eV),\\ N(^2D) + C_2H_6 &\rightarrow NH + C_2H_5\,(+1.29eV). \end{aligned} \tag{9}$$

The first two reactions in the list are also the most efficient energy producers, with energy rates integrated over altitude on the day side of 4.9×10^{-4} erg cm^{-2}s^{-1} and 4.4×10^{-4} erg cm^{-2}s^{-1}, respectively. These numbers, provided as reference values, do not strictly represent heating rates for Titan's neutral atmosphere. In particular, for reactions producing light particles, such as H or H_2, the exothermic energy is likely to be redistributed spatially in the form of kinetic energy (see section 3.4).

[37] The excited state of methylene, $^1CH_2$, is essentially produced through the photodissociation of methane and is quickly quenched by N_2 and CH_4, releasing a great amount of heat into the atmosphere:

$$^1CH_2 + N_2 \rightarrow {}^3\,CH_2 + N_2\,(+0.32eV), \tag{10}$$

$$^1CH_2 + CH_4 \rightarrow 2CH_3\,(+0.54eV). \tag{11}$$

On the day side, the integrated energy rates are 1.8×10^{-4} erg cm^{-2}s^{-1} and 1.2×10^{-4} erg cm^{-2}s^{-1} for reactions (10) and (11), respectively. On the night side, however, these mechanisms are entirely suppressed owing to the disappearance of $^1CH_2$, which is mainly a product of methane photodissociation. Two other $^1CH_2$-quenching mechanisms are taken into account in the present model, but have a smaller impact on Titan's energy balance. They involve methane and acetylene and their integrated energy rates, on the day side, are 1.4×10^{-5} erg cm^{-2}s^{-1} and 1.1×10^{-5} erg cm^{-2}s^{-1}, respectively:

$$\begin{aligned} ^1CH_2 + CH_4 &\rightarrow {}^3CH_2 + CH_4\,(+0.32eV),\\ ^1CH_2 + C_2H_2 &\rightarrow C_3H_3 + H\,(+0.87eV). \end{aligned} \tag{12}$$

[38] The N_2^+ excited states X, A, B, C, D, and $(2\sigma-1)\Sigma_g$ are considered as a result of the photoionization and electron impact ionization of nitrogen [*Gan*, 1991; *Gan et al.*, 1992]. The lifetimes of these excited states are found to be on the order of a microsecond, whereas the quenching time constant corresponding to reaction $N_2^+(A) + N_2 \rightarrow N_2^+(X) + N_2$ is on the order of a second. The N_2^+ excited states are assumed either to return into their ground state $N_2^+(X)$ by radiating away their energy, therefore remaining unavailable for heating the neutral atmosphere, or to lead to the dissociation of N_2^+ into $N(^4S, {}^2D) + N^+$, in which case energy is immediately released into the atmosphere under the form of the fragments' kinetic energy (see section 3.3).

[39] Most of the ions produced by the methane photoionization and electron impact ionization are considered in their ground states [*Gan*, 1991; *Gan et al.*, 1992]: CH_4^+ (threshold of 980 Å), CH_3^+ (880 Å), and CH_2^+ (820 Å). Only species CH^+ and H^+ are considered both in their ground states $CH^+(X)$ (560 Å) and $H^+(X)$ (555 Å), and in their excited states $CH^+(A)$ (510 Å) and $H^+(A)$ (465 Å). In the same way as for the excitation energies of N_2^+, the internal energies of $CH^+(A)$ and $H^+(A)$ are assumed to be lost to space through radiation.

3.2. Energy Produced by Exothermic Ion and Neutral Chemistry

[40] The exothermic energy produced by the ion and neutral chemical reactions are determined using the enthalpies of formation proposed by *Burcat* [2001], *Chase* [1998], *Lias et al.* [1988], and *McEwan and Phillips* [1975]. Local time-dependent energy rates are calculated by running the coupled ion-neutral rotating model of *De La Haye et al.* [2008] in the solar and latitudinal conditions of flybys T_A and T_5's closest approaches ($F10.7$ cm = 136.7 s.f.u., $F_{Av}10.7$ cm = 105.9 s.f.u., 38.8°N for T_A, and $F10.7$ cm = 82.9 s.f.u., $F_{Av}10.7$ cm = 86.0 s.f.u., 73.7°N for T_5). The electron temperature profile used to calculate electron recombination rates is that reported by *Wahlund et al.* [2005], from the measurements of the Cassini Radio and Plasma Wave Science instrument during the inbound portion of the T_A flyby. The exothermic chemical reactions are ranked according to their diurnally averaged energy rates integrated over the altitude range of the study (600 km < z < 1500 km). The top energy-producing reactions are presented in Table 3 with their integrated energy rates obtained in the T_A-run at local times 0 h and 12 h. The reactions are separated into four groups, bimolecular or termolecular neutral chemistry, ion-neutral chemistry, and electron recombination, due to their different altitude predominance. Energy rate profiles are presented in Figures 6, 7, 8, and 9, for local times 12 h and 0 h. Although only the 38 top reactions are presented in detail, the contributions of the remaining 718 reactions included by *De La Haye et al.* [2008] are also taken into account for the final heating calculations.

[41] The reaction producing the most energy in Titan's upper atmosphere is found to be:

$$H_2CN + H \rightarrow HCN + H_2\,(+3.33eV), \tag{13}$$

with peak energy rates of $\simeq 2.1 \times 10^{-10}$ erg cm^{-3}s^{-1} at 940 km on the day side (12 h), and $\simeq 4.8 \times 10^{-11}$ erg cm^{-3}s^{-1} at 910 km on the night side (0 h). The second most important reaction is:

$$CH + CH_4 \rightarrow C_2H_4 + H\,(+2.57eV), \tag{14}$$

with an energy production peak of $\simeq 1.8 \times 10^{-10}$ erg cm^{-3}s^{-1} at 825 km, local time noon. Reaction (14) is found to

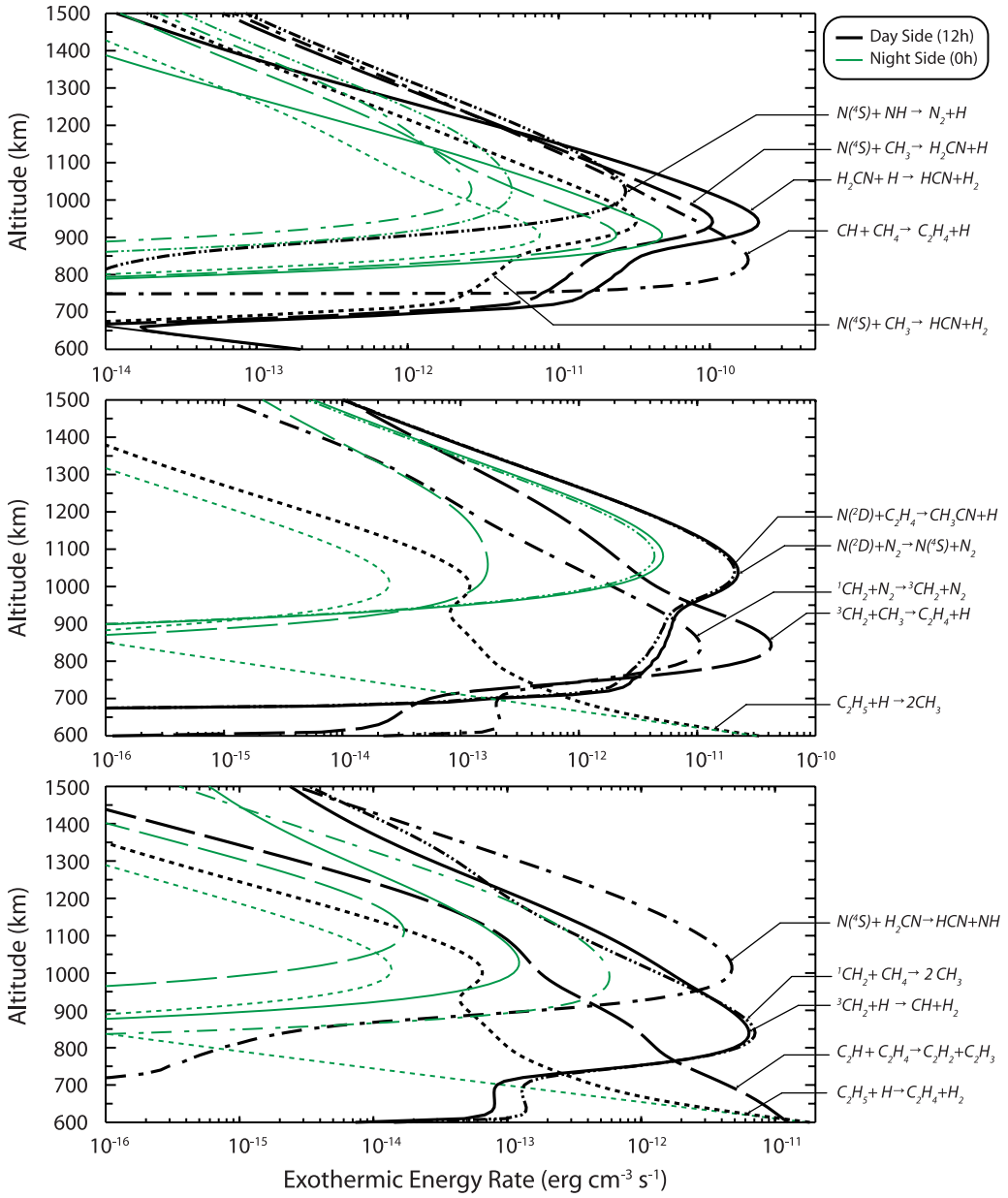

Figure 6. Exothermic energy rate produced by the most efficient bimolecular neutral reactions in Titan's upper atmosphere. Profiles corresponding to local times 12 h (black) and 0 h (green) are presented, using a specific line style for each reaction.

dominate the chemical energy production on the day side in the altitude region between 750 and 900 km. Its influence becomes much weaker on the night side with a peak energy rate about an order of magnitude smaller than that of reaction (13) at the same local time (Figure 6, top). The third bimolecular neutral reaction with an integrated energy rate larger than 10^{-3} erg cm^{-2} s^{-1} is:

$$N\left(^4S\right) + CH_3 \rightarrow H_2CN + H\,(+1.68eV), \qquad (15)$$

with a peak energy rate of $\simeq 1.0 \times 10^{-10}$ erg cm^{-3}s^{-1} at 940 km on the day side and $\simeq 2.4 \times 10^{-11}$ erg cm^{-3}s^{-1} at 910 km on the night side. It is interesting to note that equations (15) and (13) represent the main source and sink, respectively, for species H_2CN.

[42] The next most efficient chemical process for producing energy in Titan's upper atmosphere is the electron recombination of major ion H_2CN^+, which dominates, by far, other electron recombination processes:

$$H_2CN^+ + e^- \rightarrow HCN + H\,(+6.16eV). \qquad (16)$$

Its peak energy rates, $\simeq 8.5 \times 10^{-11}$ erg cm^{-3}s^{-1} at 1020 km on the day side and $\simeq 1.3 \times 10^{-11}$ erg cm^{-3}s^{-1} at 1170 km on the night side, are about an order of magnitude greater than the peak of the next electron recombination reaction (Figure 9). The day to night variation in the electron recombination energy rates is mainly due to the disappearance of photoelectrons on the night side.

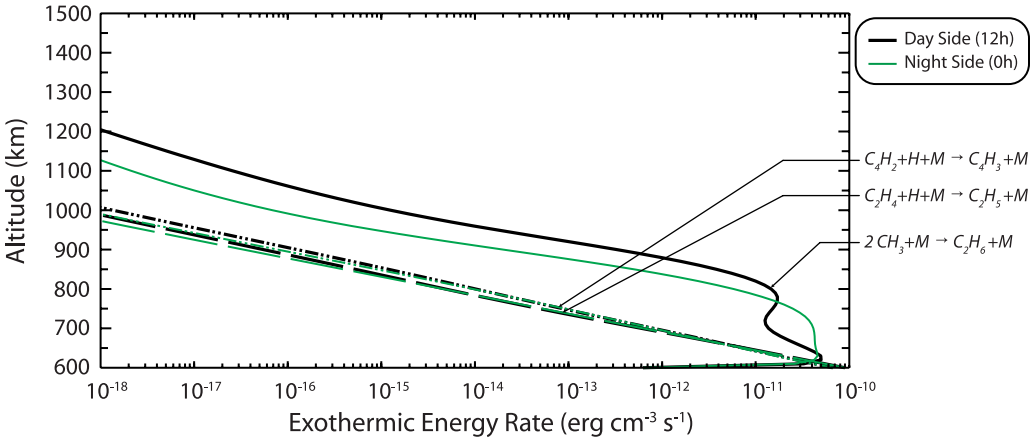

Figure 7. Exothermic energy rate produced by the most efficient termolecular neutral reactions in Titan's upper atmosphere. Profiles corresponding to local times 12 h (black) and 0 h (green) are presented, using a specific line style for each reaction.

[43] The next top two reactions are then found in the ion-neutral chemistry category:

$$CH_3^+ + CH_4 \rightarrow C_2H_5^+ + H_2\,(+1.21eV), \tag{17}$$

$$N_2^+ + CH_4 \rightarrow CH_3^+ + N_2 + H\,(+1.27eV), \tag{18}$$

with very similar energy rate profiles, peaking at 1040 km on the day side with a value of about $\simeq 2.1 \times 10^{-11}$ erg cm^{-3}s^{-1} and at 1180 km on the night side with a value of $\simeq 6.3 \times 10^{-12}$ erg cm^{-3}s^{-1} (Figure 8). At low altitudes, the most important mechanism for Titan's energy balance is the termolecular neutral reaction involving two methyl radicals and leading to the formation of ethane:

$$CH_3 + CH_3 \xrightarrow{M} C_2H_6\,(+3.84eV). \tag{19}$$

This process has an equivalent influence on the day side and on the night side (Figure 7), with peak energy rates of

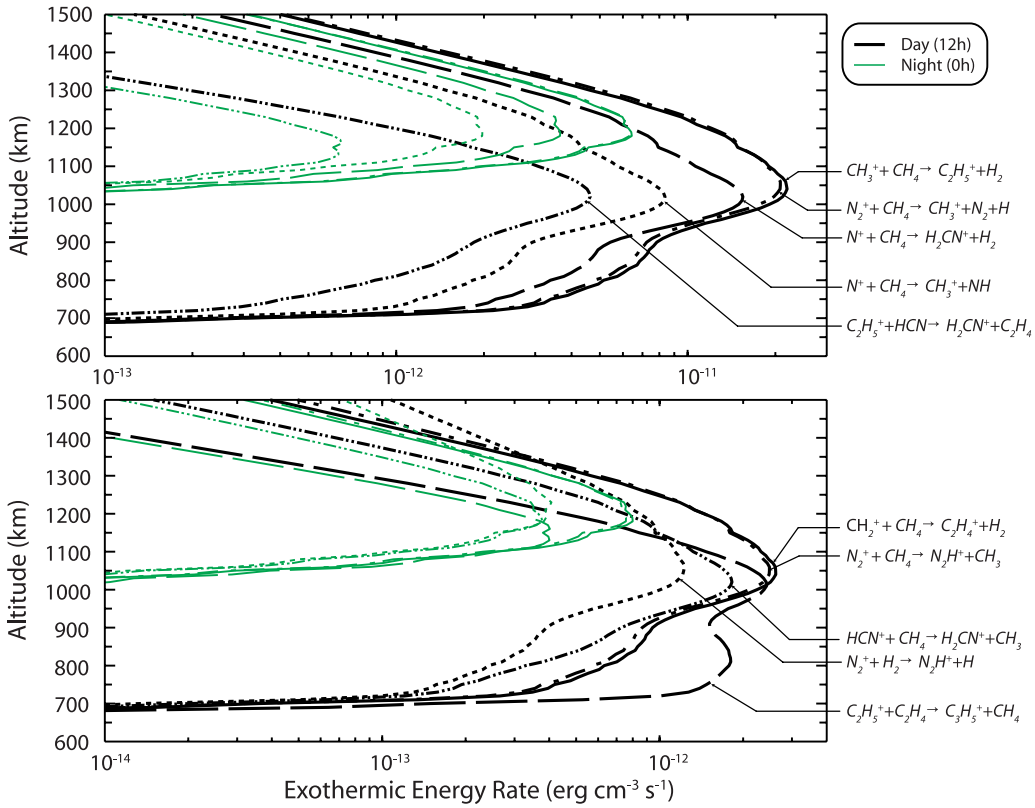

Figure 8. Exothermic energy rate produced by the most efficient ion-neutral reactions in Titan's upper atmosphere. Profiles corresponding to local times 12 h (black) and 0 h (green) are presented, using a specific line style for each reaction.

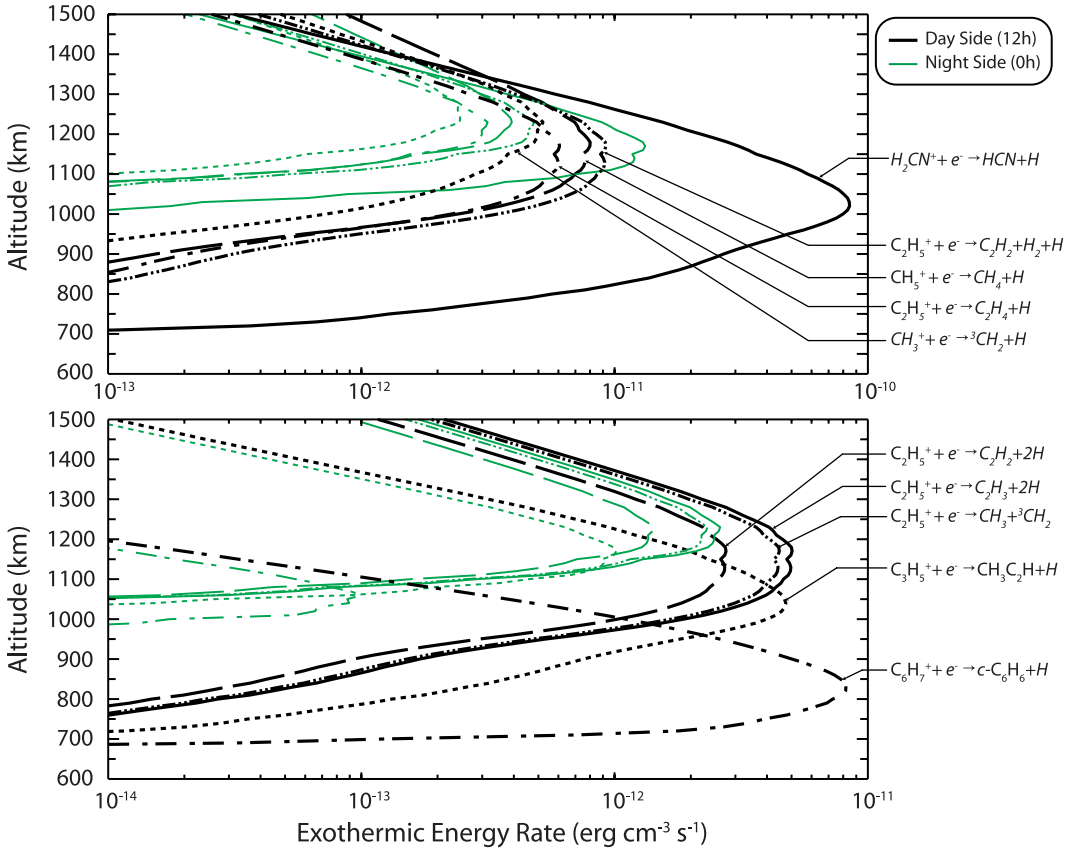

Figure 9. Exothermic energy rate produced by the most efficient electron recombination reactions in Titan's upper atmosphere. Profiles corresponding to local times 12 h (black) and 0 h (green) are presented, using a specific line style for each reaction.

$\simeq 5.0 \times 10^{-11}$ erg cm^{-3}s^{-1} at 620 km (12 h) and $\simeq 4.6 \times 10^{-11}$ erg cm^{-3}s^{-1} at 630 km (0 h).

3.3. Kinetic Energy of Fragments Resulting From Photodissociation, Photoionization, and Electron Impact Dissociation and Ionization

[44] Kinetic energy is directly released into Titan's upper atmosphere as a result of the photoionization, photodissociation, and electron impact ionization and dissociation of N_2:

$$N_2 + h\nu, e^- \rightarrow N^+ + N + K.E., \quad (20)$$

$$\rightarrow N + N + K.E. \quad (21)$$

An approximation of the corresponding energy rate is calculated assuming that each nitrogen atom is attributed a kinetic energy of 1 eV after electron impact (a value corresponding to the peak energy distributions reported by *Cosby* [1993] and *Ajello and Ciocca* [1996]) and 0.5 eV after photodissociation and photoionization (a value corresponding to the center of the main peak of the energy distribution evaluated by *Bakalian* [2006]). The corresponding energy rate profiles are plotted in Figure 10 for local times noon and midnight, using the ionization and dissociation rates of *De La Haye et al.* [2008] for the T_A run. Peak kinetic energy rates are found for atomic nitrogen at $\simeq$1050 km (day side) and 1250 km (night side), representing <8% and <5% of the energy produced by exothermic chemistry at those altitude, respectively. The kinetic energy of fragments resulting from methane dissociation is neglected in the present work (CH_4 mixing ratio of 3–4% at 1200 km in the work of *De La Haye et al.* [2008]), with a contribution assumed to be minor compared to that of nitrogen and lying within the uncertainties involved in the present calculations.

[45] The altitude-dependent energy productions of bimolecular or termolecular neutral chemistry, ion-neutral chemistry, and electron recombination are also compared in Figure 10. Bimolecular neutral chemistry is found to dominate the energy balance by about an order of magnitude between 700 and 1100 km on the day side and between 850 and 1100 km on the night side, with peaks at 950 km and 900 km, respectively. Below this altitude range, whether on the day side or on the night side, termolecular neutral chemistry becomes dominant, increasing with decreasing altitude, until it reaches the lower boundary at 600 km. Above 1100 km, electron recombination reactions become the major energy producer in Titan's upper atmosphere, consistently followed by ion-neutral chemistry with energy rate values about twice lower. These two mechanisms peak at 1025 km, observe a local depletion at about 900 km, and become insignificant below 700 km.

Table 3. Top Exothermic Chemical Reactions in Titan's Upper Atmosphere, Ranked by Integrated Energy Rates Averaged Over a Titan Day[a]

	Reaction			$\Delta_r H^\circ$ (*eV*)	Q_{12h} (in erg cm^{-2} s^{-1})	Q_{0h}
			Bimolecular Neutral Reactions			
1	$H_2CN + H$	$\rightarrow$	$HCN + H_2$	3.33	3.3×10^{-3}	6.1×10^{-4}
2	$CH + CH_4$	$\rightarrow$	$C_2H_4 + H$	2.57	3.1×10^{-3}	5.6×10^{-5}
3	$N(^4S) + CH_3$	$\rightarrow$	$H_2CN + H$	1.68	1.7×10^{-3}	3.2×10^{-4}
4	$N(^4S) + CH_3$	$\rightarrow$	$HCN + H_2$	5.01	5.3×10^{-4}	9.8×10^{-5}
5	$N(^4S) + NH$	$\rightarrow$	$N_2 + H$	6.54	5.1×10^{-4}	1.2×10^{-4}
6	$N(^2D) + N_2$	$\rightarrow$	$N(^4S) + N_2$	2.38	4.9×10^{-4}	8.9×10^{-5}
7	$N(^2D) + C_2H_4$	$\rightarrow$	$(CH_3CN) + H$	2.43	4.4×10^{-4}	7.6×10^{-5}
8	$^3CH_2 + CH_3$	$\rightarrow$	$C_2H_4 + H$	2.69	5.8×10^{-4}	4.4×10^{-6}
9	$C_2H_5 + H$	$\rightarrow$	$CH_3 + CH_3$	0.48	8.0×10^{-5}	6.1×10^{-5}
10	$^1CH_2 + N_2$	$\rightarrow$	$^3CH_2 + N_2$	0.32	1.8×10^{-4}	0
11	$C_2H + C_2H_4$	$\rightarrow$	$C_2H_2 + C_2H_3$	0.44	1.2×10^{-4}	2.8×10^{-7}
12	$N(^4S) + H_2CN$	$\rightarrow$	$HCN + NH$	2.08	8.6×10^{-5}	1.2×10^{-5}
13	$H + {}^3CH_2$	$\rightarrow$	$H_2 + CH$	0.11	1.2×10^{-4}	2.3×10^{-6}
14	$^1CH_2 + CH_4$	$\rightarrow$	$CH_3 + CH_3$	0.54	1.2×10^{-4}	0
15	$C_2H_5 + H$	$\rightarrow$	$C_2H_4 + H_2$	2.94	4.3×10^{-5}	3.3×10^{-5}
			Termolecular Neutral Reactions			
1	$CH_3 + CH_3$	$\xrightarrow{M}$	C_2H_6	3.84	5.1×10^{-4}	6.6×10^{-4}
2	$C_2H_4 + H$	$\xrightarrow{M}$	C_2H_5	1.55	1.8×10^{-4}	1.8×10^{-4}
3	$C_4H_2 + H$	$\xrightarrow{M}$	C_4H_3	1.80	1.5×10^{-4}	1.4×10^{-4}
			Ion-Neutral Reactions			
1	$CH_3^+ + CH_4$	$\rightarrow$	$C_2H_5^+ + H_2$	1.21	7.1×10^{-4}	1.3×10^{-4}
2	$N_2^+ + CH_4$	$\rightarrow$	$CH_3^+ + N_2 + H$	1.27	6.9×10^{-4}	1.3×10^{-4}
3	$N^+ + CH_4$	$\rightarrow$	$H_2CN^+ + H_2$	8.91	4.6×10^{-4}	7.8×10^{-5}
4	$N^+ + CH_4$	$\rightarrow$	$CH_3^+ + NH$	3.47	2.5×10^{-4}	4.2×10^{-5}
5	$C_2H_5^+ + HCN$	$\rightarrow$	$H_2CN^+ + C_2H_4$	0.41	1.2×10^{-4}	1.1×10^{-5}
6	$CH_2^+ + CH_4$	$\rightarrow$	$C_2H_4^+ + H_2$	2.54	8.5×10^{-5}	1.6×10^{-5}
7	$N_2^+ + CH_4$	$\rightarrow$	$N_2H^+ + CH_3$	2.62	8.2×10^{-5}	1.6×10^{-5}
8	$C_2H_5^+ + C_2H_4$	$\rightarrow$	$C_3H_5^+ + CH_4$	0.87	8.2×10^{-5}	6.5×10^{-6}
9	$N_2^+ + H_2$	$\rightarrow$	$N_2H^+ + H$	2.63	4.6×10^{-5}	1.1×10^{-5}
10	$HCN^+ + CH_4$	$\rightarrow$	$H_2CN^+ + CH_3$	2.93	5.3×10^{-5}	7.4×10^{-6}
			Electron Recombination Reactions			
1	$H_2CN^+ + e-$	$\rightarrow$	$HCN + H$	6.16	2.0×10^{-3}	2.4×10^{-4}
2	$C_2H_5^+ + e-$	$\rightarrow$	$C_2H_2 + H_2 + H$	4.81	2.7×10^{-4}	9.9×10^{-5}
3	$CH5^+ + e-$	$\rightarrow$	$CH_4 + H$	7.87	2.5×10^{-4}	9.6×10^{-5}
4	$C_2H_5^+ + e-$	$\rightarrow$	$C_2H_4 + H$	6.57	1.8×10^{-4}	6.4×10^{-5}
5	$CH_3^+ + e-$	$\rightarrow$	$^3CH_2 + H$	5.10	1.5×10^{-4}	5.5×10^{-5}
6	$C_2H_5^+ + e-$	$\rightarrow$	$C_2H_3 + 2H$	2.18	1.5×10^{-4}	5.3×10^{-5}
7	$C_2H_5^+ + e-$	$\rightarrow$	$CH_3 + {}^3CH_2$	3.88	1.3×10^{-4}	4.7×10^{-5}
8	$C_2H_5^+ + e-$	$\rightarrow$	$C_2H_2 + 2\ H$	2.56	8.0×10^{-5}	2.9×10^{-5}
9	$C_6H_7^+ + e-$	$\rightarrow$	$c\text{-}C_6H_6 + H$	8.45	1.5×10^{-4}	1.0×10^{-6}
10	$C_3H_5^+ + e-$	$\rightarrow$	$CH_3C_2H + H$	5.64	1.0×10^{-4}	1.6×10^{-5}

[a] $\Delta_r H^\circ$, enthalpy of reaction; Q_{12h}, rate of energy produced by the exothermic chemical reactions, integrated over the entire altitude range at noon; Q_{0h}, rate of energy produced by the exothermic chemical reactions, integrated over the entire altitude range at midnight. Note: The ranks were assigned on the basis of sets of results for 12 local times. Therefore there is no systematic correspondence between the ranks and the sum of the energy rate integrated values at 12 h and 0 h.

3.4. Redistribution of Exothermic Heat by Suprathermal Neutrals

[46] The excess of energy resulting from the exothermic chemical reactions is shared between the resulting fragments in the form of either kinetic energy, with the possibility of the fragments becoming suprathermal, or internal energy, i.e., electronic, vibrational, or rotational excitation. The energy carried by suprathermal neutral particles is eventually released into the atmosphere through a cascade of collisions with the background gas. However, the energy release might not occur immediately or in the region of formation of the initial suprathermal particles. In addition, in some cases, particles with sufficient energy reaching the exobase might escape and thus be lost to the neutral atmosphere from a heating point of view. So to determine the contribution of exothermic chemical reactions to heating Titan's upper atmosphere, it is necessary to estimate first the energy redistribution and loss by travel and escape of suprathermal chemical fragments.

[47] The transport of suprathermal neutrals is modeled using the two stream model of *De La Haye et al.* [2007b], based on the work of *Nagy and Cravens* [1981, 1988]. The suprathermal particles are considered to lose energy solely via collisions with the cold ambient neutral gas. Inelastic processes are assumed to be negligible owing to the low enough energy of the suprathermal particles (<10 eV). All collisions, considered to be elastic, are modeled using the hard sphere assumption. This assumption implies that the energy dependence of elastic collision cross sections is neglected, and that heat loss mechanisms, such as radiation, are ignored. This study therefore represents an overestimate of the heat actually released into Titan's upper atmosphere.

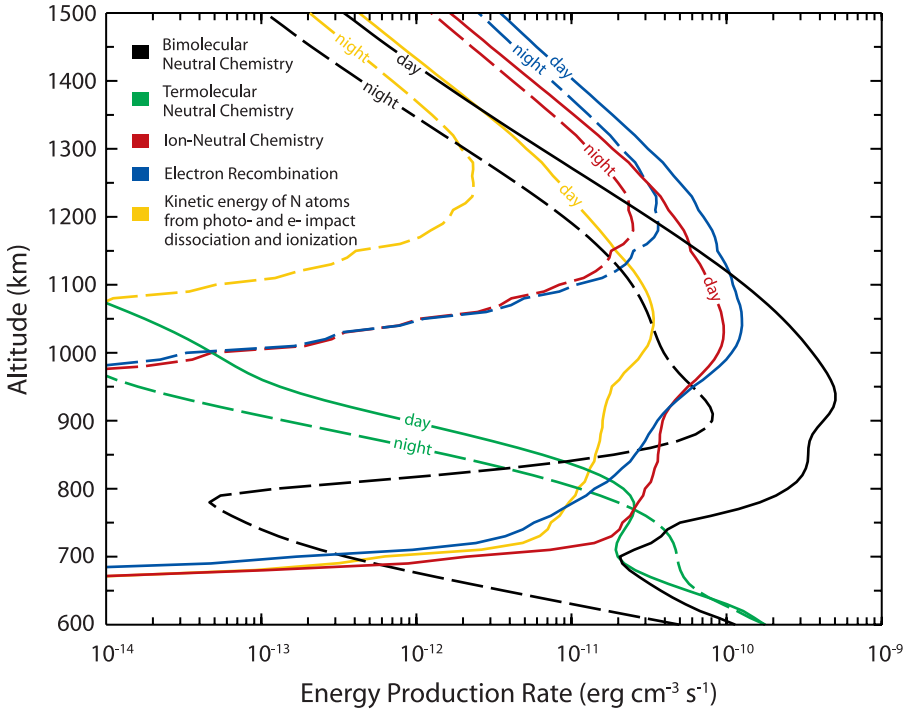

Figure 10. Rate of the energy produced by exothermic chemical reactions in Titan's upper atmosphere: comparative altitude influence of neutral bimolecular chemistry (black), neutral termolecular chemistry (green), ion-neutral chemistry (red), and electron recombination (blue). Kinetic energy rates of fragments resulting from photodissociation, photoionization, and electron impact dissociation and ionization are plotted in yellow. Profiles corresponding to local times 12 h (solid lines) and 0 h (dash lines) are presented.

Let's consider that a collision between a suprathermal particle with energy E and a background particle with thermal energy E_b results in a suprathermal particle with energy $E' = E\text{-}\Delta E$ and a background particle with energy $E_b' = E_b + \Delta E$. For each collision, the model distinguishes the following events: (1) the suprathermal particle cascades to another suprathermal level ($E' > thermal$), (2) the suprathermal particle becomes thermal ($E' = thermal$), (3) the background particle is hit by sufficient energy and becomes suprathermal ($E_b' > thermal$), and (4) the background particle remains thermal ($E_b' = thermal$). The portion of the collisional energy, ΔE, involved in events 2 and 4 is considered to contribute as heat to the neutral atmosphere. Further description of the two stream model, including formulas, is given by *De La Haye et al.* [2007b]. The conservation of energy is verified at each given altitude by checking that energy loss and gain remain equal between z − dz/2 and z + dz/2.

[48] As done by *De La Haye et al.* [2007b], the possibility of the neutrals N_2, CH_4, H, H_2, $^3CH_2$, CH_3, C_2H_4, C_2H_5, C_2H_6, $N(^4S)$, NH, and HCN being produced in a suprathermal form is examined. The suprathermal particles' production rates are calculated for the appropriate local time and latitude using the composition model of *De La Haye et al.* [2008]. The results of various runs of the two-stream model are presented in Figure 11 to compare the influence of each of these fast neutrals on the energy redistribution. The background gas, for all two-stream simulations, is assumed to be a thermal mixture of N_2, CH_4, and H_2. First, a nominal case is examined by simultaneously modeling fast neutrals N_2, CH_4, and H_2 as they travel through the background mixture of thermal N_2, CH_4, and H_2. New runs are then performed by adding separately one of the other considered fast neutrals to the nominal run. For example, to test the influence of fast neutral H, the results obtained by modeling fast neutrals N_2, CH_4, H_2, and H as simultaneously traveling through the background mixture of N_2, CH_4, and H_2 are examined. The corresponding heat redistribution ratio profiles, i.e., the ratio between the heat actually released into the thermal atmosphere and the total energy initially produced by the exothermic chemical reactions, are plotted in Figure 11.

[49] When fast neutrals N_2, CH_4, and H_2 are modeled alone, species H_2 is largely responsible for the heat redistribution due to its light weight (black round markers in Figure 11). The corresponding heat redistribution ratio shows a minimum value of $\simeq$0.8 at 950 km, corresponding to the large amounts of suprathermal H_2 molecules produced at that altitude. In addition, the local depletion observed at $\simeq$1400 km is due to the important escape flux of the hot H_2 molecules crossing the exobase in the upward direction with energy >4.6 × 10^{-2} eV. The H_2 escape flux, induced by exothermic chemistry, was calculated to be 1.3 × 10^7 cm^{-2} s^{-1} [*De La Haye et al.*, 2007b].

[50] The comparison of the results from the other simulations show a dominating influence of species H over most of the study's altitude range (red solid line compared to black solid line in Figure 11). Its energy redistribution

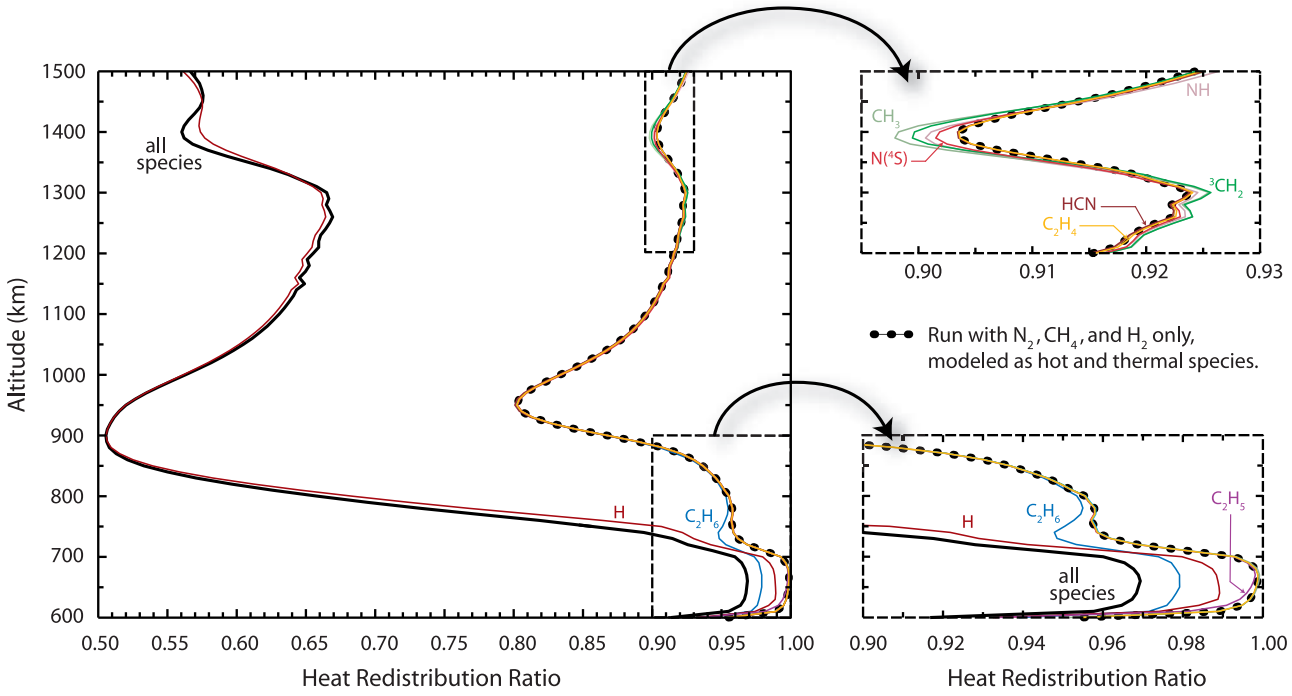

Figure 11. Heat redistribution ratios obtained by separately modeling hot populations of H, $^3CH_2$, CH_3, C_2H_4, C_2H_6, $N(^4S)$, NH, and HCN, traveling through a background mixture of N_2, CH_4, and H_2. The hot components of the background species are taken into account each time. Result profiles are also presented for the hot N_2, CH_4, and H_2 alone (round black markers) and for all the aforementioned hot species simultaneously (solid black line).

influence has a similar shape to that of H_2, but with a greater amplitude due to its lighter weight and greater velocity. Two main depletions are observed in the heat redistribution ratio profile: at 900 km ($\simeq$0.51), an altitude region where highly energetic hydrogen atoms are formed and from which they are likely to travel away, and at 1400 km ($\simeq$0.575) due to atomic hydrogen escape. All hot hydrogen atoms reaching the exobase are likely to escape, since the H-escape energy is 2.2×10^{-2} eV at the exobase.

[51] At altitudes lower than 800 km, the C_2H_6 hot component becomes the dominant factor in the heat-redistribution ratio (blue solid line in Figure 11). This effect is mainly due to reaction $CH_3 + CH_3 \xrightarrow{M} C_2H_6$, which produces ethane molecules with energy 1.86 eV. Owing to the heavy weight of the hot C_2H_6 molecules, the cascading process is slow and thermalization is delayed. A portion of the chemical exothermic energy is kept in the C_2H_6 suprathermal population, inducing a depletion of $\simeq$0.02 at 650 km in the heat redistribution ratio. A similar process takes place for hot C_2H_5 particles due to reaction $C_2H_4 + H \xrightarrow{M} C_2H_5$, but its effect on the heat redistribution ratio (<0.003) is limited compared to the aforementioned process.

[52] The influence of the other hot species on heat redistribution is found to remain within 1% of the total exothermic chemical energy. Their added influence, however, is non-negligible, in particular around 1400 km where the heat redistribution ratios exhibit a simultaneous depletion due to the escape of energetic particles. With these considerations in mind, various simulations are performed, simultaneously modeling all the suggested fast neutrals, to cover the local-times and zenith angle ranges of the T_A and T_5 simulations.

[53] The main uncertainty in the model is in the determination of the fast neutrals' production rates, and especially in the assumption here that 100% of the chemical exothermic energy is transferred to the reaction products in the form of kinetic energy. The influence of this assumption on the heat redistribution was tested by running test results with only 50% of the exothermic energy being transferred as kinetic energy and 50% transferred as internal excitations and immediately restituted as heat into the thermal atmosphere. The difference between the resulting heating rate profiles was found to be maximal at 900 km, with a heating rate about 50% greater when using the 50%-assumption compared to the 100%-assumption. These differences are attributed mainly to the H and H_2 particles traveling with lower velocity with the 50%-assumption, and therefore transporting less energy throughout the atmosphere, thus also inferring less energy escape. This significant effect suggests the need for further studies on internal excitations of fragments resulting from exothermic chemical reactions. However, since internal excitation, such as vibration, could also lead to radiation, and therefore to the energy being lost from the neutral atmosphere, the 100%-assumption was judged appropriate to provide a first evaluation of the heating efficiencies in Titan's upper atmosphere.

3.5. Results: Local Time-Dependent Heating Rates Induced by Exothermic Chemistry

[54] The heating rates induced by exothermic chemistry after heat redistribution by suprathermal particles are pre-

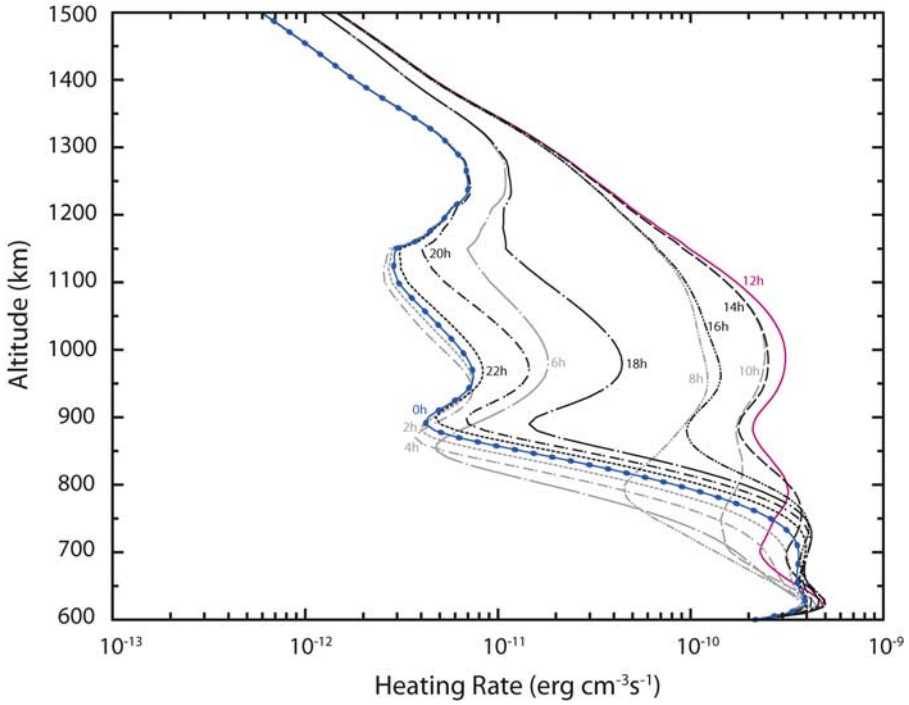

Figure 12. Local time-dependent heating rates induced by exothermic chemistry in the solar conditions of the T_A flyby at a fixed latitude of 38.8° North. The effects of both photoelectrons and magnetospheric electrons are taken into account.

sented in Figure 12 for the solar conditions of the T_A flyby, at latitude 38.8° North, and for twelve local times covering a Titan day from noon (12 h) to midnight (0 h) and from midnight to noon. The subsolar latitude remains at $\simeq$23° South. The heating profiles are found to weaken from day side to night side, showing an interesting pattern of local peak change in number and altitude. Three local peaks are observed at noon: (1) 620 km, (2) 790 km, and (3) 990 km. The first local peak remains present at the same altitude for all local times, with a small amplitude variation reaching a minimum at 4 h local time. The second local peak progressively increases in amplitude while decreasing in altitude between 12 h and 18 h, where it reaches a value of $\simeq 4.2 \times 10^{-10}$ erg cm^{-3}s^{-1} at 730 km. This peak then progressively disappears between 20 h and 8 h, and only starts reforming at local time 10 h with a value of $\simeq 1.9 \times 10^{-10}$ erg cm^{-3}s^{-1} at 820 km. The third local peak remains fairly constant in altitude throughout the range of local times, but varies by more than an order of size in amplitude. These three series of local peaks are produced by solar-driven chemistry and heat redistribution. A fourth series of local peaks appears on the night side, between 18 h and 6 h, at altitudes around 1235 km. Their amplitudes range between $\simeq 7.0 \times 10^{-12}$ erg cm^{-3}s^{-1} at 18 h and $\simeq 1.2 \times 10^{-11}$ erg cm^{-3}s^{-1} at midnight. These peaks result from heating by exothermic chemistry induced by magnetospheric electrons. They only become noticeable on the night side, while the relative effects of solar-driven mechanisms decrease.

[55] The chemistry-induced heating rates obtained in the T_5 solar and latitudinal conditions are compared to the T_A results in Figure 13. Between 600 and 700 km, the T_A heating rates are found to dominate those of T_5 by more than an order of magnitude for all local times, mainly owing to the stronger solar flux used in the T_A simulation, i.e., $F/F_{Av}10.7$ cm = 136.7/105.9 s.f.u., compared to $F/F_{AV}10.7$ cm = 82.9/86.0 s.f.u. for T_5. At higher altitudes, the T_A-heating rates remain greater on the day side, but become comparable to those of T_5 as local time shifts toward the night side. This is due to the T_A simulation, rotating at fixed latitude, encountering a stronger solar exposure on the day side but weaker exposure on the night side than T_5: zenith angles of 61.7° (12 h), 104.2° (6 h, 18 h), and 164.8° (0 h) at 38.8° N for T_A, compared to 97.0° (12 h), 112.1° (6 h, 18 h), and 129.0° (0 h) at 73.7° N for T_5. These results show the importance of considering a rotating regime, depending on latitude and local time, to determine the amount of heat received by the atmosphere during its periodic rotation with Titan.

4. Results and Discussion: Heating Rates and Heating Efficiency Profiles in Titan's Upper Atmosphere

4.1. Heating Rate Profiles

[56] The total effective heating rate in Titan's upper atmosphere is plotted for local times 12 h, 18 h, 0 h, and 6 h in Figure 14, as the sum of (1) the heating produced by electron impact after elastic collisions and internal excitations of N_2 and CH_4, (2) the heating due to suprathermal electron heating, produced by Coulomb collisions between the suprathermal electrons traveling throughout Titan's upper atmosphere and the thermal electrons, and (3) the heating produced by exothermic chemical reactions, after redistribution of a portion of the exothermic energy by suprathermal particles.

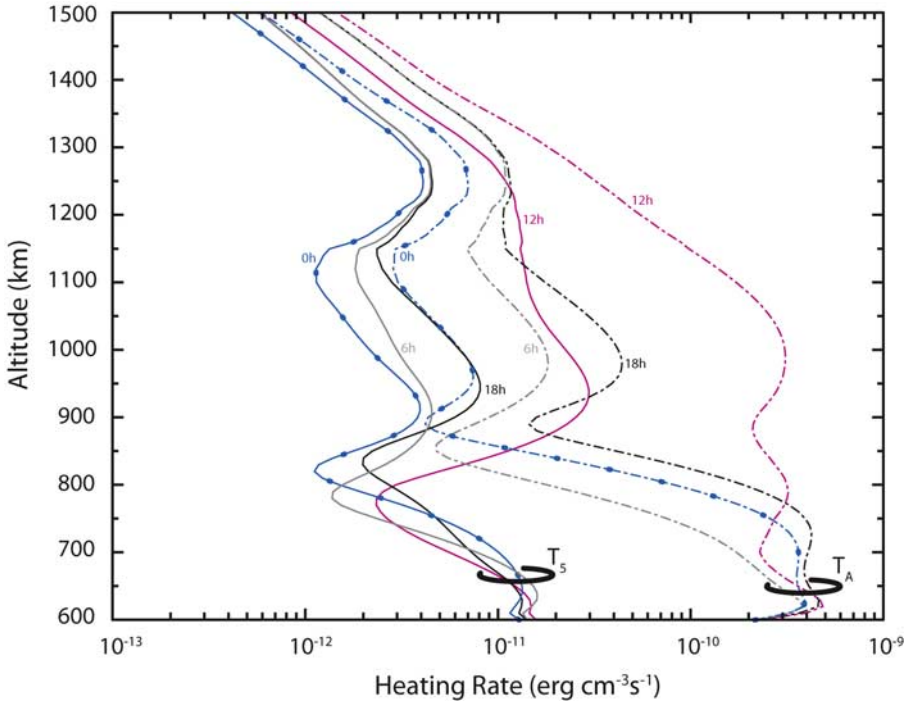

Figure 13. Comparison of the heating rates induced by exothermic chemistry in the T_A and T_5 solar and latitudinal conditions. The effects of both photoelectrons and magnetospheric electrons are taken into account.

[57] While exothermic chemistry is found to be the dominant source of heat throughout Titan's upper atmosphere, electron-impact excitation and suprathermal electron heating cannot be neglected. In the T_A simulation, their influence on the total heating rate becomes noticeable at altitudes higher than 710 km at 12 h and 1080 km at 0 h. Their relative importance becomes maximal at $\simeq$1230 km, where their combined heating represents $\simeq$50% (12 h) and $\simeq$80% (0 h) of the heating by exothermic chemistry.

[58] In Figure 14, heating rates are compared to the cooling rate produced by the radiative emissions of the *HCN* rotational lines, which was identified by *Yelle* [1991] as the major coolant at altitudes greater than 700 km. The cooling rate was determined by using a radiative transfer calculation at low altitudes, assuming Local Thermodynamic Equilibrium (LTE) and a parallel plane atmosphere, and the cool-to-space approximation at high altitudes. The local time-dependent results of *De La Haye et al.* [2008] were used for the HCN mixing ratios.

4.2. Heating Efficiency Profiles

[59] Calculating heating efficiencies require the heating rate at a given altitude to be divided by the total energy absorbed/deposited at that altitude. The energy deposited by solar radiation was determined as the total photon energy absorbed by the neutrals, while photons are progressing downward into Titan's upper atmosphere. For magnetospheric electrons, the energy deposited at a given altitude is more difficult to determine than for photons. We approximate the total energy deposition rate at a given altitude by multiplying the ionization rate due to magnetospheric electron precipitation (as calculated by *De La Haye et al.* [2008]) by a mean energy loss per ion pair (about 40 eV per ion pair, the approximation used by *Waite et al.* [1983]). This provides a denominator for the heating efficiency calculation.

[60] Diurnal averages of the energy deposition are compared to the total heating rates in Figure 15 (top) for the T_A and T_5 simulations, when taking into account or neglecting the contribution of magnetospheric electrons. Solar absorption is found to be the dominating energy source below $\simeq$1150 km, and the contribution of magnetospheric electrons becomes significant above. The corresponding heating efficiency profiles are presented in Figure 15 (bottom), with values varying greatly with altitude, ranging between 10 and 40% in the T_A flyby conditions, and between 2 and 42% in the T_5 flyby conditions. At altitudes >1150 km, the heating efficiencies for the solar contribution only become factors of 1.5 to 2 times greater compared to those for the combined solar and magnetospheric contributions. This variation is mainly due to the absence of the magnetospheric energy deposition term in the denominator of the heating efficiency ratio. Heating efficiencies are presented as diurnal average only since energy deposited by solar radiation becomes close to zero on the night side. The central value of the T_A heating efficiency profile, 25 ± 15%, is consistent with the value 27 ± 5% estimated by *Fox and Yelle* [1991] for the 800–1300 km altitude range.

4.3. Thermal Structure

[61] In order to provide a first estimate of the effects of local time-varying heating on the temperature profile, a one-dimensional thermal structure model is constructed on the basis of the heat transfer equation, taking into account thermal conduction, solar and magnetospheric heating as described in the present study, and LTE emissions of the

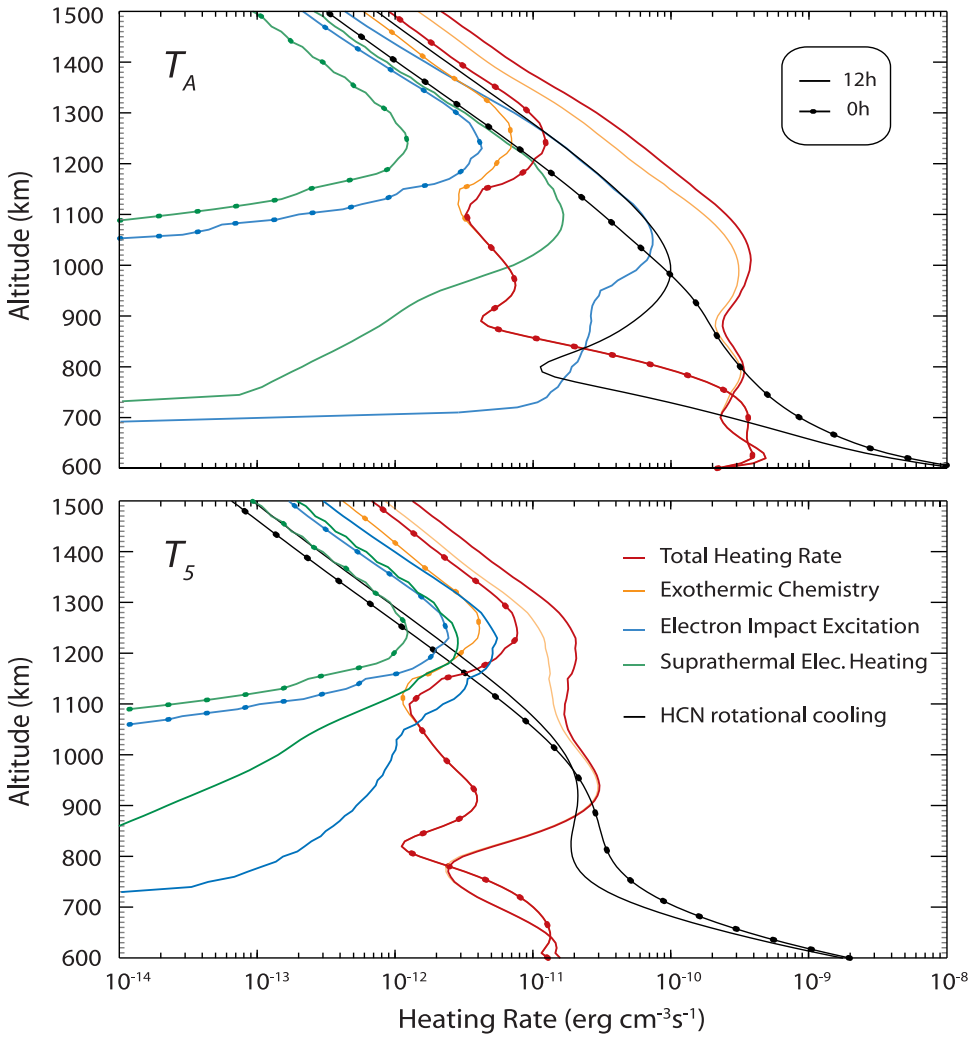

Figure 14. Heating rate profiles resulting from exothermic chemistry (orange), excitation of N_2 and CH_4 by electron impact (blue), and suprathermal electron heating (green). Results are presented for local times noon (solid lines) and midnight (solid lines with markers) corresponding to the solar and latitudinal conditions of flybys (top) T_A and (bottom) T_5.

HCN rotational lines. The time scales of Titan's thermal structure were shown to be comparable to Titan's rotational period by *De La Haye et al.* [2008]. The same rotating method as that of the *De La Haye et al.* [2008] composition model is applied. The present 1D-thermal structure model goes through an array of zenith angles corresponding to local time variation at constant latitude (38.8°N for T_A and 73.7°N for T_5), while advancing toward equilibrium. Periodic equilibrium is found to be reached after 90 Titan days. It is important to note that the present one-dimensional rotating thermal structure model is only presented to illustrate the previously calculated heating rates. There is no pretense of this model accurately describing Titan's thermal structure, especially since it does not take into account 3D dynamic processes, shown to play an important role at Titan [*Müller-Wodarg et al.*, 2006, 2008].

[62] The resulting local time-dependent temperature profiles, assuming a fixed boundary condition of 160 K at 600 km, are presented in Figure 16 for the T_A and T_5 simulations. The exospheric temperatures were found to vary between 127.9 K at 6 h local time and 156.3 K at 18 h local time in the T_A case, and between 143.6 K at 4 h local time and 149.1 K at 14 h local time in the T_5 case. The diurnal temperature variation is found to be five times larger in the T_A case, 28.4 K, compared to the T_5 case, 5.5 K. These findings are related to the zenith angle variation being $\simeq$3.2 times larger during a rotation at the T_A latitude, 61.7° at noon to 164.8° at midnight, compared to a rotation at the T_5 latitude, 97.0° at noon to 129.0° at midnight. The diurnal variation found in the T_A simulation is about 3.5 and 1.5 times greater than the temperature differences of 8 K and 18 K, calculated with the global three dimensional model of *Müller-Wodarg et al.* [2000] at solar minimum and maximum, respectively. The discrepancy between these results may be partially due to the one-dimensional limitations of the present model, where horizontal dynamics are not taken into account.

[63] The diurnally averaged exospheric temperatures obtained with the present model are 142.0 K (T_A simulation) and 145.9 K (T_5 simulation). These values are about 11 K

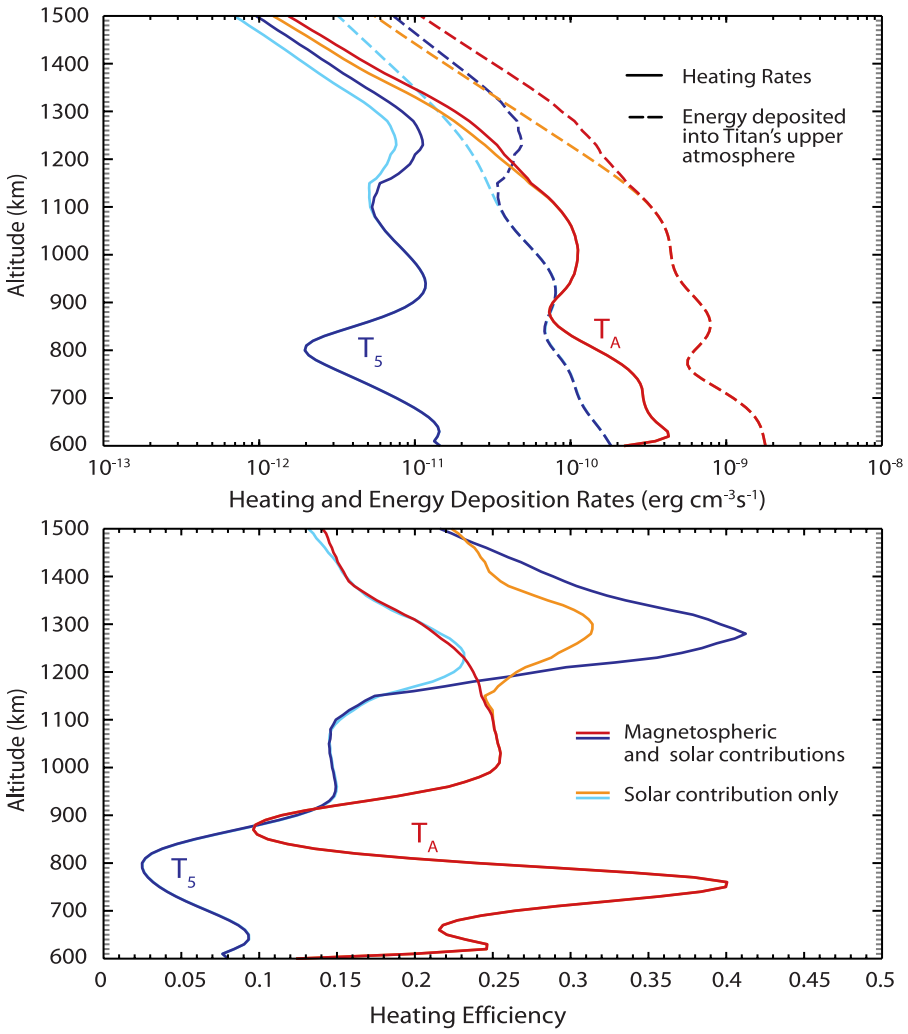

Figure 15. (top) Diurnally averaged profiles of the heating rates (strong lines) and energy deposition rates (dash lines). (bottom) Diurnally averaged profiles of the heating efficiencies. Results are presented by considering the solar and latitudinal conditions of flybys T_A (reddish colors) and T_5 (bluish colors). The solar contribution is considered either alone (orange and cyan) or combined with the magnetospheric contribution (red and blue).

lower than the temperatures of 152.8 K and 157.4 K obtained by fitting the T_A and T_5 INMS data, respectively [*De La Haye et al.*, 2007a]. It was pointed out by *De La Haye et al.* [2007a] that the relatively lower temperature obtained from fitting the T_A INMS data as compared to fitting the T_5 data is a trend opposite to the effects expected from solar-driven mechanisms. (The T_A flyby occurred near the dusk terminator whereas the T_5 flyby occurred on the night side. Additionally, the solar radiation was greater during T_A compared to T_5.) The same trend is noted here; the average of the modeled exospheric temperatures is lower for the T_A as compared to the T_5 simulation. This result is found to be a direct product of the rotating simulation method at constant latitude, with the T_A simulation (latitude of 38.8°N) encountering a stronger solar exposure on the day side but weaker exposure on the night side as compared to T5 (latitude of 73.7°N). One must also note that the T_A simulation is subject to a greater cooling rate than T_5, owing to the greater *HCN* abundance used [see *De La Haye et al.*, 2008, Figure 24]. This contribution is limited, however, since an opposite trend is obtained when the model is run using the same parameters but in a fixed local-time mode. In the latter case, the following exospheric temperatures are found: 196.0 K for T_A (fixed zenith angle 61.7°, solar radiation $F/F_{Av}10.7$ cm = 136.7/105.9 s.f.u.) and 178.4 K for T_5 (fixed zenith angle 97.0°, solar radiation $F/F_{AV}10.7$ cm = 82.9/86.0 s.f.u.). These results draw the attention to the importance of local time and latitudinal effects in modeling heating rates and temperature in Titan's upper atmosphere, especially considering that the order of magnitude of the thermal structure time scale is comparable to Titan's rotational period. It must be pointed out that the recent 3D empirical study of *Müller-Wodarg et al.* [2008], describing the mean state of Titan's thermosphere on the basis of the latest INMS data (flybys T_5 to T_{32}), presented a latitudinal trend opposite to that above, with a temperature decreasing with increasing latitude. Again, the one-dimensional rotating thermal structure model is not meant to substitute for 3D methods, and is only used to illustrate the heating rate results of the present paper, using the two specific config-

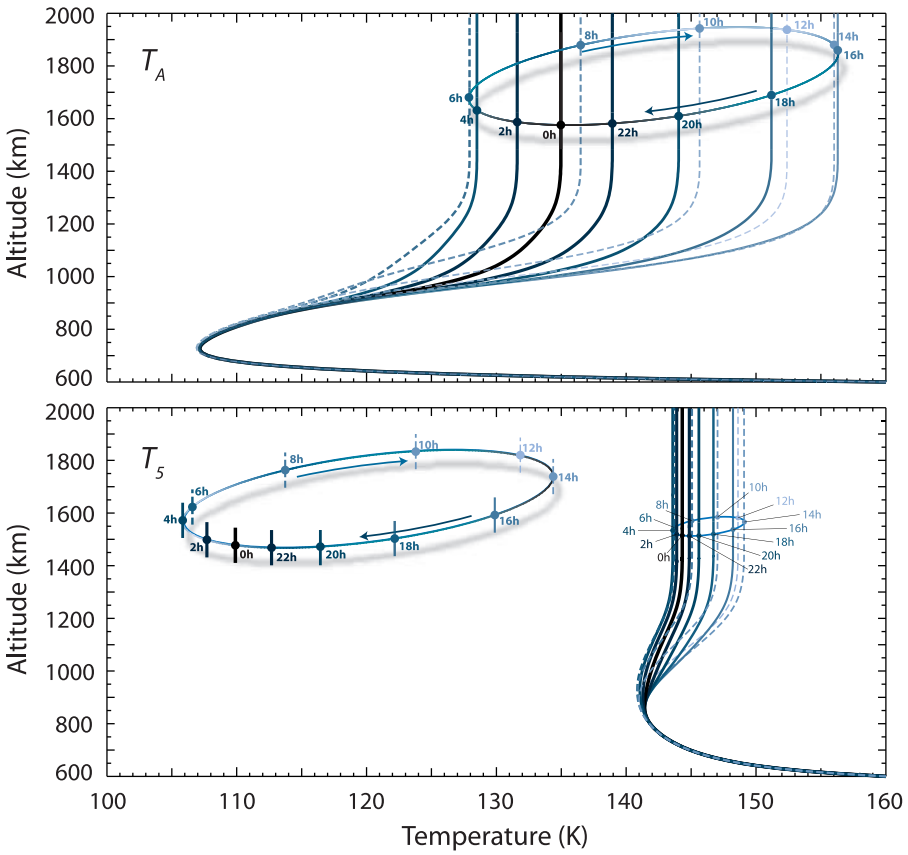

Figure 16. Local time-dependent temperature profiles estimated using a thermal structure rotating model, taking into account thermal conduction, *HCN* rotational cooling, and the present study's heating rates. Results are presented in the solar and latitudinal conditions of flybys (top) T_A and (bottom) T_5.

urations of solar radiation and ion-neutral composition corresponding to flybys T_A and T_5.

[64] A temperature minimum, that would correspond to the presence of a mesopause, is found at 730 km in the T_A case (107 K) and at 920 km in the T_5 case (141 K). These values are 46 K and 16 K lower than the temperatures recommended in the T_A and T_5 reference profiles of *De La Haye et al.* [2008], determined using the CIRS and the INMS data and presenting no mesopause configuration. These observations underscore the limitations of the present thermal structure model, suggesting, in particular, the overestimation of the *HCN* rotational cooling rate at low altitudes (Figure 14). These limitations may be due to various factors, including the limited information available on the *HCN* density profile in Titan's atmosphere and the omission in the present model of heat sources operative below 600 km, for example, the absorption by C_2H_6 of radiation emitted by the warm stratosphere as suggested by *Yelle* [1991]. Further study on the internal properties of complex hydrocarbon and nitrile molecules are needed to offer a better understanding of the cooling and heating processes taking place in Titan's upper atmosphere.

5. Conclusions

[65] The present work offers a thorough analysis of the heating mechanisms of Titan's neutral upper atmosphere, including electron impact excitation of nitrogen and methane, suprathermal electron heating, and ion-neutral exothermic chemistry. The contributions of solar photons and Saturn's magnetospheric electrons were both taken into account.

[66] Exothermic chemistry was found to be the dominant source of heat, with electron-impact excitation and suprathermal electron heating becoming significant above $\simeq$700 km on the day side (zenith angle of $\simeq$60°) and $\simeq$1100 km on the night side (zenith angle of $\simeq$165°). The most energetic exothermic chemical reactions were identified and classified, and their energy production rates were presented as a function of altitude and local time. Five photochemical processes were distinguished: bimolecular neutral chemistry, which dominates between 700 and 1100 km on the day side and between 850 and 1100 km on the night side, termolecular neutral chemistry, dominating below, ion-neutral chemistry and electron recombination reactions, dominating above, and fragments' kinetic energy from N_2 ionization and dissociation, about an order of magnitude smaller. Some of the fragments produced by photochemistry were found to be suprathermal, vertically redistributing heat throughout Titan's upper atmosphere. A two stream model was used to model the heat redistribution. The hot hydrogen atoms and molecules were found to be the main contributors for transporting the initial exothermic energy.

[67] Local time-dependent heating rate profiles were presented, corresponding to the solar conditions and fixed

latitude of the T_A and T_5 flybys' closest approach. Significant variations were found over a Titan day in the altitude and amplitude of the local peak heating. The largest amplitude variation was obtained in the T_A simulation, with a value of $\simeq 3 \times 10^{-10}$ erg cm^{-3}s^{-1} at 990 km and $\simeq 7 \times 10^{-12}$ erg cm^{-3}s^{-1} at 940 km, corresponding to zenith angles of 62° and 165°, respectively. Diurnally averaged heating efficiency profiles were presented, showing large altitude variations. Values of 25 ± 15% and 23 ± 19% were calculated, corresponding to the T_A and T_5 simulations, respectively. These results are in good agreement with the heating efficiency of 27 ± 5% reported by *Fox and Yelle* [1991].

[68] Local time-dependent temperature profiles were also estimated using a rotating 1D-thermal structure model, taking into account thermal conduction, LTE cooling of the HCN rotational lines, and the calculated heating rates. The exospheric temperature, diurnally averaged, was found to be greater in the T_5 simulation (146 K) compared to the T_A simulation (142 K), despite the weaker solar radiation and greater zenith angle at noon used to reproduce the T_5 solar conditions. This trend was found to be opposite to that of a fixed local time calculation at noon, underscoring the importance of latitudinal and local time variations. The present one-dimensional rotating model remains, however, limited as it does not take into account dynamic processes, which are important factors in Titan's upper atmosphere, as evidenced by the presence of waves [*Müller-Wodarg et al.*, 2006] and winds [*Müller-Wodarg et al.*, 2008].

[69] The present study underscores the limits of previous global circulation models [e.g., *Müller-Wodarg et al.*, 2000], especially in their use of parameterized heating efficiencies, often approximated to a constant value with respect to both altitude and local time. To allow an adequate estimate of local time-dependent heating by solar photons and magnetospheric electrons, we suggest, instead of heating efficiencies, the inclusion into future 3D models of a simplified ion and neutral chemical scheme such as that presented by *De La Haye et al.* [2008]. Owing to computational cost, however, heating redistribution by suprathermal neutrals may have to be taken into account using altitude-dependent parameterized factors.

[70] Further studies are also necessary to better understand the heating and cooling mechanisms that take place in the lower part of the present study's altitude range. These studies should focus on the radiative properties of the complex hydrocarbon species present in Titan's upper atmosphere at a molecular level.

[71] **Acknowledgments.** This research was supported by the NASA Jet and Propulsion Laboratory contract 1283095, NASA task order NMO710023, Support INMS Instrument on Cassini Spacecraft During Tour. The authors thank R. V. Yelle of the University of Arizona for his input.

[72] Wolfgang Baumjohann thanks Valery Shematovich and another reviewer for their assistance in evaluating this paper.

References

Agren, K., et al. (2007), On magnetospheric electron impact ionization and dynamics in Titan's ram-side and polar ionosphere-A Cassini case study, *Ann. Geophys.*, *25*, 2359–2369.

Ajello, J. M., and M. Ciocca (1996), Fast nitrogen atoms from dissociative excitation of N_2 by electron impact, *J. Geophys. Res.*, *101*, 18,953–18,960.

Bakalian, F. (2006), Production of hot nitrogen atoms in the Martian thermosphere, *Icarus*, *183*, 69–78.

Brescansin, L. M., M. A. P. Lima, and V. McKoy (1989), Cross sections for rotational excitation of CH_4 by 3–20 eV electrons, *Phys. Rev. A*, *40*, 5577–5582.

Burcat, A. (2001), Third millennium ideal gas and condensed phase thermochemical database for combustion, *Rep. 867*, Technion Aerosp. Eng., Haifa, Israel.

Cartwright, D. C., S. Trajmar, A. Chutjian, and W. Williams (1977), Electron impact excitation of the electronic states of N_2. II. Integral cross sections at incident energies from 10 to 50 eV, *Phys. Rev. A*, *16*, 1041–1051.

Chamberlain, J. W. (1961), *Physics of the Aurora and Airglow*, Academic, New York.

Chase, M. W. (1998), *NIST-JANAF Thermochemical Tables*, 4th ed., *J. Phys. Chem. Ref. Monogr.*, vol. 9, Springer, New York.

Coates, A. J., F. J. Crary, D. T. Young, K. Szego, C. S. Arridge, Z. Bebesi, E.C. Sittler Jr., R.E. Hartle, and T.W. Hill (2007), Ionospheric electrons in Titan's tail: Plasma structure during the Cassini T9 encounter, *Geophys. Res. Lett.*, *34*, L24S05, doi:10.1029/2007GL030919.

Cosby, P. C. (1993), Electron-impact dissociation of nitrogen, *J. Chem. Phys.*, *98*, 9544–9553.

Cravens, T. E., I. P. Robertson, S. A. Ledvina, D. Mitchell, S. M. Krimigis, and J. H. Waite Jr. (2008), Energetic ion precipitation at Titan, *Geophys. Res. Lett.*, *35*, L03103, doi:10.1029/2007GL032451.

De La Haye, V., et al. (2007a), Cassini Ion and Neutral Mass Spectrometer data in Titan's upper atmosphere and exosphere: Observation of a suprathermal corona, *J. Geophys. Res.*, *112*, A07309, doi:10.1029/2006JA012222.

De La Haye, V., J. H. Waite Jr., T. E. Cravens, A. F. Nagy, R. V. Yelle, R. E. Johnson, S. Lebonnois, and I. P. Robertson (2007b), Titan's corona: The contribution of exothermic chemistry, *Icarus*, *191*, 236–250, doi:10.1016/j.icarus.2007.04.031.

De La Haye, V., J. H. Waite Jr., T. E. Cravens, I. P. Robertson, and S. Lebonnois (2008), Coupled ion and neutral rotating model of Titan's upper atmosphere, *Icarus*, *197*(1), 110–136, doi:10.1016/j.icarus.2008.03.022.

Eastes, R. W., and A. V. Dentamaro (1996), Collision-induced transitions between the $a^1\pi_g$, $a'^1\sigma_u^-$, and $w^1\delta_u$ states of N_2: Can they affect auroral N_2 Lyman-Birge-Hopfield band emissions?, *J. Geophys. Res.*, *101*, 26,931–26,940.

Fox, J. L. (1988), Heating efficiencies in the thermosphere of Venus reconsidered, *Planet. Space Sci.*, *36*, 37–46.

Fox, J. L., and R. V. Yelle (1991), Solar heating efficiencies in the thermosphere of Titan, *Bull. Am. Astron. Soc.*, *23*, 1184.

Friedson, A. J., and Y. L. Yung (1984), The thermosphere of Titan, *J. Geophys. Res.*, *89*, 85–90.

Galand, M., R. V. Yelle, A. J. Coates, H. Backes, and J.-E. Wahlund (2006), Electron temperature of Titan's sunlit ionosphere, *Geophys. Res. Lett.*, *33*, L21101, doi:10.1029/2006GL027488.

Gan, L. (1991), Electron distributions and solar wind interaction with nonmagnetic planets, Ph.D. thesis, Univ. of Michigan, Ann Arbor.

Gan, L., and T. E. Cravens (1992), Electron impact cross sections and cooling rates for methane, *Planet. Space Sci.*, *40*, 1535–1544.

Gan, L., C. N. Keller, and T. E. Cravens (1992), Electrons in the ionosphere of Titan, *J. Geophys. Res.*, *97*, 12,136–12,151.

Gan, L., T. E. Cravens, and C. N. Keller (1993), A time-dependent model of suprathermal electrons at Titan, in *Plasma Environments of Non-Magnetic Planets*, edited by T. I. Gombosi, Pergamon, New York.

Gilmore, F. R., R. R. Laher, and P. J. Espy (1992), Franck-Condon factors, r-centroids, electronic transition moments and Einstein coefficients for many nitrogen and oxygen band systems, *J. Phys. Chem. Ref. Data*, *21*, 1005–1107.

Green, A. E. S., and S. K. Dutta (1967), Semi-empirical cross sections for electron impacts, *J. Geophys. Res.*, *72*, 3933–3941.

Green, A. E. S., and T. Sawada (1972), Ionization cross sections and secondary electron distributions, *J. Atmos. Terr. Phys.*, *34*, 1719–1728.

Herzberg, G. (1945), *Molecular Spectra and Molecular Structure: II. Infrared and Raman Spectra of Polyatomic Molecules*, Van Nostrand, New York.

Herzberg, G. (1950), *Molecular Spectra and Molecular Structure. I. Spectra of Diatomic Molecules*, Van Nostrand Reinhold, New York.

Itikawa, Y., M. Hayashi, A. Ichimura, K. Onda, K. Sakimoto, K. Takayanagi, M. Nakamyura, H. Nishimura, and T. Takayanagi (1986), Cross sections for collisions of electrons and photons with nitrogen molecules, *J. Phys. Chem. Ref. Data*, *15*, 985–1010.

Jain, A. (1986), Total (elastic + absorption) cross sections for e-CH_4 collisions in a spherical model at 0.10–500 eV, *Phys. Rev. A*, *34*, 3707.

Jain, A., and D. G. Thomson (1983), Rotational excitation of CH_4 and H_2O by slow electron impact, *J. Phys. B. At. Mol. Phys.*, *16*, 3077–3098.

Katayama, D. H., A. V. Dentamaro, and J. A. Welsh (1994), State specific electronic quenching rates for the N_2 $a^1\pi_g$ ($v' = 0$) level from collisions with He, Ar, and N_2, *J. Chem. Phys.*, *101*, 9422–9428.

Khristenko, S. V., A. I. Maslov, and V. P. Shevelko (1998), *Molecules and Their Spectroscopic Properties*, Springer, New York.

Ledvina, S. A., and T. E. Cravens (1998), A single fluid three-dimensional model of plasma flow around Titan, *Planet. Space Sci.*, *46*, 1175–1191.

Lias, S. G., J. E. Bartness, J. F. Liebman, J. L. Holmes, R. D. Levin, and W.G. Mallard (1988), Gas-phase ion and neutral thermochemistry, *J. Phys. Chem. Ref. Data*, *17*, 1988.

Lin, C. L., and F. Kaufman (1971), Reactions of metastable nitrogen atoms, *J. Chem. Phys.*, *55*, 3760–3770.

Ma, Y.-J., A. F. Nagy, T. E. Cravens, I. V. Sokolov, J. Clark, and K. C. Hansen (2004), 3-D global MHD model prediction for the first close flyby of Titan by Cassini, *Geophys. Res. Lett.*, *31*, L22803, doi:10.1029/2004GL021215.

Marinelli, W. J., W. J. Kessler, B. D. Green, and W. A. M. Blumberg (1989), Quenching of N_2 ($a^1\pi_g$, $v' = 0$) by N_2, O_2, CO, CO_2, CH_4, H_2, and Ar, *J. Chem. Phys.*, *90*, 2167–2173.

McEwan, J. M., and L. F. Phillips (1975), *Chemistry of the Atmosphere*, Halsted, New York.

Michael, M., and R. E. Johnson (2005), Energy deposition of pickup ions and heating of Titan's atmosphere, *Planet. Space Sci.*, *53*, 263–267.

Millet, P., Y. Salamero, H. Brunet, J. Galy, D. Blanc, and J. L. Teyssier (1973), De-excitation of N_2 ($c^3\pi_u$, $v' = 0$ and 1) levels in mixtures of oxygen and nitrogen, *J. Chem. Phys.*, *58*, 5839–5841.

Morrill, J. S., and W. M. Benesh (1996), Auroral N_2 emissions and the effect of collisional processes on N_2 triplet state vibrational populations, *J. Geophys. Res.*, *101*, 261–274.

Muller, R., K. Jung, K.-H. Kochem, W. Sohn, and H. Ehrhardt (1985), Rotational excitation of CH_4 by low-energy-electron collisions, *J. Phys. B At. Mol. Phys.*, *18*, 3971–3985.

Müller-Wodarg, I. C. F., R. V. Yelle, L. A. Young, and A. D. Aylward (2000), The thermosphere of Titan simulated by a global three-dimensional time-dependent model, *J. Geophys. Res.*, *105*, 20,833–20,856.

Müller-Wodarg, I. C. F., R. V. Yelle, N. Borggren, and J. H. Waite Jr. (2006), Waves and horizontal structures in Titan's thermosphere, *J. Geophys. Res.*, *111*, A12315, doi:10.1029/2006JA011961.

Müller-Wodarg, I. C. F., R. V. Yelle, J. Cui, and J. H. Waite (2008), Horizontal structures and dynamics of Titan's thermosphere, *J. Geophys. Res.*, *113*, E10005, doi:10.1029/2007JE003033.

Nagy, A. F., and P. M. Banks (1970), Photoelectron fluxes in the ionosphere, *J. Geophys. Res.*, *75*, 6260–6270.

Nagy, A. F., and T. E. Cravens (1981), Hot oxygen atoms in the upper atmosphere of Venus, *Geoph. Res. Lett.*, *8*, 629–632.

Nagy, A. F., and T. E. Cravens (1988), Hot oxygen atoms in the upper atmosphere of Venus and Mars, *Geoph. Res. Lett.*, *15*, 433–435.

Neubauer, F. M., D. A. Gurnett, J. D. Scudder, and R. E. Hartle (1984), Titan's magnetospheric interaction, in *Saturn*, edited by T. Gehrels and M. S. Matthews, pp. 760–787, Univ of Ariz. Press, Tucson.

Orient, O. J., and S. K. Srivastava (1987), Electron impact ionization of H_2O, CO, CO_2, and CH_4, *J. Phys. B*, *20*, 3923–3936.

Piper, L. G. (1987), Quenching rate coefficients for N_2 ($a'^1\sigma_u^-$), *J. Chem. Phys.*, *87*, 1625–1629.

Piper, L. G. (1992), Energy transfer studies on N_2 ($x^1\sigma_g^+$, v) and N_2 ($b^3\pi_g$), *J. Chem. Phys.*, *97*, 270–275.

Roble, R. G., E. C. Ridley, and R. E. Dickinson (1987), On the global mean structure of the thermosphere, *J. Geophys. Res.*, *92*, 8745–8758.

Schunk, R. W., and A. F. Nagy (2000), *Ionospheres: Physics, Plasma Physics, and Chemistry*, Cambridge Univ. Press, Cambridge, U.K.

Shimamura, I. (1983), Patial-sum rules for and asymmetry between rotational transitions $J \pm \Delta J \leftarrow J$, *Phys. Rev. A*, *28*, 1357–1362.

Shyn, T. W., and T. E. Cravens (1990), Angular distribution of electrons elastically scattered from CH_4, *J. Phys. B At. Mol. Opt. Phys.*, *23*, 293–300.

Sohn, W., K. Jung, and H. Ehrhardt (1983), Threshold structures in the cross sections of low-energy electron scattering of methane, *J. Phys. B At. Mol. Phys.*, *16*, 891–901.

Solomon, S. C., P. B. Hays, and V. J. Abreu (1988), The auroral 6300 Å emission: Observations and modeling, *J. Geophys. Res.*, *93*, 9867.

Susskind, J. (1973), Analysis of the ν_4 band of CH_4, *J. Mol. Spectrosc.*, *45*, 457–466.

Tanaka, H., M. Kubo, N. Onodera, and A. Suzuki (1983), Vibrational excitation of CH_4 by electron impact: 3–20 eV, *J. Phys. B. At. Mol. Phys.*, *16*, 2861–2869.

Torr, M. R., P. G. Richards, and D. G. Torr (1980), A new determination of the ultraviolet heating efficiency of the thermosphere, *J. Geophys. Res.*, *85*, 6819–6826.

Trajmar, S., D. F. Register, and A. Chutjian (1983), Electron scattering by molecules II. Experimental methods and data, *Phys. Rep.*, *97*, 219–356.

Vroom, D. A., and F. J. de Heer (1969), Production of excited hydrogen atoms by impact of fast electrons on some simple hydrocarbons, *J. Chem. Phys.*, *50*, 573–579.

Vuskovic, L., and S. Trajmar (1983), Electron impact excitation of methane, *J. Chem. Phys.*, *78*, 4947–4951.

Wahlund, J.-E., et al. (2005), Cassini measurements of cold plasma in the ionosphere of Titan, *Science*, *308*, 986–989.

Waite, J. H., Jr., T. E. Cravens, J. Kozyra, A. F. Nagy, S. K. Atreya, and R. H. Chen (1983), Electron precipitation and related aeronomy of the Jovian thermosphere and ionosphere, *J. Geophys. Res.*, *88*, 6143–6163.

Waite, J. H., Jr., et al. (2005), Ion neutral mass spectrometer results from the first flyby of Titan, *Science*, *308*, 982–986.

Wilson, E. H., and S. K. Atreya (2004), Current state of modeling the photochemistry of Titan's mutually dependent atmosphere and ionosphere, *J. Geophys. Res.*, *109*, E06002, doi:10.1029/2003JE002181.

Yelle, R. V. (1991), Non-LTE models of Titan's upper atmosphere, *Astrophys. J.*, *383*, 380–400.

Yung, Y. L., M. Allen, and J. P. Pinto (1984), Photochemistry of the atmosphere of Titan: Comparison between model and observations, *Astrophys. J. Suppl. Ser.*, *55*, 465–506.

Zipf, E. C., and R. W. McLaughlin (1978), On the dissociation of nitrogen by electron impact and by E.U.V. photo-absorption, *Planet. Space Sci.*, *26*, 449–462.

Zipf, E. C., P. J. Espy, and C. F. Boyle (1980), The excitation and collisional deactivation of metastable N (^{2}P) atoms in auroras, *J. Geophys. Res.*, *85*, 687–694.

J. M. Bell, V. De La Haye, and J. H. Waite Jr., Southwest Research Institute, 6220 Culebra Road, San Antonio, TX 78228, USA. (hunter.waite@swri.org)

S. W. Bougher, Department of Atmospheric, Oceanic and Space Sciences, University of Michigan, Ann Arbor, MI 48109, USA.

T. E. Cravens and I. P. Robertson, Department of Physics and Astronomy, University of Kansas, Lawrence, KS 66045, USA.